Case Studies in Thermal Engineering 74 (2025) 106846

Contents lists available at ScienceDirect

Case Studies in Thermal Engineering

journal homepage: www.elsevier.com/locate/csite

# Three-dimensional thermomechanical modeling of geothermal energy piles with U-tube heat exchangers of different cross-sectional shapes

Samia Boudjaza [a,b], Abdelmadjid Chehhat [a,c], Abdelmadjid Kaddour [d], Younes Menni [e,f,*], Samia Larguech [g], Badr M. Alshammari [h], Lioua Kolsi [i,**]

[a] Department of Mechanical Engineering, Faculty of Science and Technology, University of Khenchela, 40000, Khenchela, Algeria
[b] Laboratory of Engineering and Science of Advanced Materials (ISMA), University of Khenchela, 40000, Khenchela, Algeria
[c] LESEI Laboratory, University of Batna 2, Batna, 05000, Algeria
[d] Unité de Recherche Appliquée en Energies Renouvelables, URAER, Centre de Développement des Energies Renouvelables, CDER, 47133, Ghardaïa, Algeria
[e] Department of Mechanical Engineering, Institute of Technology, University Center Salhi Ahmed Naama (Ctr. Univ. Naama), P.O. Box 66, Naama, 45000, Algeria
[f] College of Technical Engineering, National University of Science and Technology, Dhi Qar, 64001, Iraq
[g] Department of Electrical Engineering, College of Engineering, Princess Nourah bint Abdulrahman University, P.O. Box 84428, Riyadh, 11671, Saudi Arabia
[h] Department of Electrical Engineering, College of Engineering, University of Ha'il, Ha'il City, 81451, Saudi Arabia
[i] Department of Mechanical Engineering, College of Engineering, University of Ha'il, Ha'il City, 81451, Saudi Arabia

ARTICLE INFO

*Keywords:*
Geothermal energy pile
Thermomechanical analysis
Heat exchanger geometry
Thermal performance
Energy foundation systems

ABSTRACT

This study explores the thermomechanical performance of a three-dimensional (3D) geothermal energy pile (GEP) system, emphasizing the optimization of heat exchanger (HE) geometry to improve both thermal efficiency and structural integrity. As GEPs offer a promising avenue for integrating renewable geothermal energy into building foundations, their design must balance energy performance with mechanical stability. A finite volume-based numerical model is developed, employing second-order spatial and temporal discretization and the Pressure-Implicit with Splitting of Operators (PISO) algorithm for pressure–velocity coupling. A segregated solution strategy with under-relaxation is used to ensure numerical stability and convergence. The model simulates a concrete-encased U-shaped HE embedded in clayey soil, with three cross-sectional geometries: circular, square, and triangular. Simulation outcomes are validated against analytical predictions and benchmarked with experimental and numerical data from the literature. Among the tested geometries, the triangular HE demonstrates superior thermal and structural performance under both mechanical and thermomechanical loading conditions. Compared to the circular configuration, the triangular U-pipe enhances cooling efficiency by reducing outlet temperature by 1.2 % and increasing heat extraction by 8.6 %. In heating mode, it raises the outlet temperature by 0.6 % but lowers the heat transfer rate by 4.8 %, underscoring the need for season-specific or hybrid designs. Thermomechanically, the triangular configuration exhibits the highest axial compressive stress in summer, increasing by 6.36 %, while in winter, it shows a 4.75

* Corresponding author.Department of Mechanical Engineering, Institute of Technology, University Center Salhi Ahmed Naama (Ctr. Univ. Naama), P.O. Box 66, Naama, 45000, Algeria.
** Corresponding author.
*E-mail addresses:* menni.younes@cuniv-naama.dz (Y. Menni), l.kolsi@uoh.edu.sa (L. Kolsi).

https://doi.org/10.1016/j.csite.2025.106846
Received 29 April 2025; Received in revised form 19 July 2025; Accepted 7 August 2025
Available online 9 August 2025

% reduction relative to the purely mechanical load case. Displacement variations at the pile base remain minimal across all geometries, with the triangular HE showing a 1.13 % reduction in summer and a 1.70 % increase in winter. These findings establish the triangular cross-section as the most effective configuration for enhancing both thermal output and structural resilience in GEP systems, providing a valuable design reference for the development of energy-efficient, geothermal-integrated foundations.

## 1. Introduction

The contemporary energy landscape is characterized by an urgent need to transition away from conventional carbon-based energy sources, such as petroleum, coal, and natural gas, toward cleaner and more sustainable alternatives. Although these traditional fuels continue to dominate global energy supply, they account for more than two-thirds of total $CO_2$ and greenhouse gas emissions [1]. Their finite availability and detrimental environmental effects have prompted intensified efforts by governments and researchers to advance renewable energy technologies. This challenge is particularly acute in regions with rapidly increasing energy demands. For example, Algeria's electricity consumption reached a record 19,500 MW on July 21, 2024 [2], highlighting the nation's pressing need for alternative energy systems that can provide reliable and efficient performance.

Among the various renewable energy systems, geothermal energy (GE) stands out for its ability to provide continuous heat extraction from the earth's subsurface, making it particularly suitable for space heating and cooling applications [3,4]. Geothermal energy piles (GEPs), also known as thermo-active foundations, have emerged as a hybrid solution that combines the structural foundation of buildings with ground heat exchange technology. These systems employ closed-loop circuits composed of high-density polyethylene (HDPE) tubes embedded within structural foundation piles. A heat-carrying fluid (HCF) circulates through the loop, enabling heat transfer (HT) between the building structure and the surrounding soil. This process supports energy-efficient space heating during cold seasons and effective thermal regulation during warmer periods [5–7].

Extensive research on GEPs has been carried out using in-situ field experiments, scaled physical models, and numerical simulations [8–12]. A substantial portion of these studies has focused on evaluating the thermal performance of GEP systems, optimizing heat exchanger (HE) configurations, and analyzing the coupled soil–structure–thermal interactions. Zhao et al. [13] conducted a comprehensive comparative analysis of U-shaped, W-shaped, and spiral ground HEs using transient thermal simulations. Their results demonstrated that spiral-shaped HEs offer superior short-term and long-term thermal efficiency, owing to their larger HT surface area and more uniform temperature distribution. Similarly, Li et al. [14] integrated experimental observations with numerical simulations to examine temperature evolution within GEPs. Their findings indicated that spiral configurations produced more uniform and elevated temperature distributions, with soil thermal conductivity and pile diameter being critical factors. For instance, a 200 mm increase in pile diameter resulted in a 1 °C decrease in internal pile temperature over a 7-day heating period. Farajollahi et al. [15] extended this line of investigation by developing a 3D computational fluid dynamics (CFD) model of a GEP incorporating a triple-helix ground HE. Their model revealed a 24 % performance improvement over conventional designs, particularly under variations in helix pitch and pipe–soil interaction parameters.

The influence of surrounding soil properties on thermal performance was highlighted by Rui and Soga [16], who conducted an in-situ analysis of a 23 m-long GEP installed at Lambeth College. Their study identified soil thermal conductivity and the mechanical stiffness of the soil during reloading and swelling as critical determinants of system efficiency. Additionally, the thermal expansion of concrete was found to significantly affect pile head displacement, whereas soil plasticity played a lesser role due to the over-consolidated nature of London Clay. Cecinato and Salciarini [17] investigated the performance of micro-GEPs and found that pipe diameter had a more pronounced effect on HT in these systems compared to standard-sized energy piles. Furthermore, effective thermal insulation of the basement and high soil thermal conductivity were shown to enhance the long-term thermal response. Seokjae et al. [18] examined cast-in-place GEPs equipped with steel pipe HEs. Based on field tests and numerical simulations, they concluded that increasing the number of steel pipes did not necessarily improve thermal efficiency. Instead, material thermal conductivity and the optimization of flow rate, specifically 11.35 L/min for their configuration, were identified as more critical factors for enhancing system performance.

Park et al. [19] conducted thermal response tests (TRTs) for various buried pipe configurations to examine the impact of thermal interference among adjacent HEs. Their field measurements demonstrated that, while GEPs exhibited greater thermal efficiency per unit length of borehole compared to conventional borehole HEs, closely spaced installations suffered from reduced performance due to thermal interference. Based on their simulations, a design chart was developed to help mitigate these effects during system installation. In a related study, Mehrizi et al. [20] performed simulations to evaluate the performance of U-type, W-type, and all-around W-type pile foundation HEs within the context of a ground-coupled heat pump operating in cooling mode. Among the tested configurations, the all-around W-type design proved to be the most efficient, offering enhanced HT performance. The study also found that serial connections of pile HEs outperformed parallel arrangements due to more stable and consistent fluid temperature profiles.

Several researchers have investigated the use of phase change materials (PCMs) to enhance the thermal buffering capacity of GEPs. Shahidi et al. [21] examined the integration of lauric acid as a PCM in energy piles, specifically targeting applications in hot climates. Their findings revealed a significant reduction in temperature fluctuations, by 13 % in dry soil and 10 % in saturated conditions. The study also reported a substantial decrease in excess pore water pressure, indicating that thermal cycling improved the mechanical resilience of the system under heat-induced stresses. Guo et al. [22] evaluated full-scale pre-tensioned high-strength concrete (PHC)

GEPs and reported heat exchange efficiencies of 81.3 W/m in summer and 61.9 W/m in winter. An intermittent operation mode resulted in a 9.2 % improvement in HT and a 4 % increase in energy efficiency ratio compared to continuous operation. Liu et al. [23] designed a spiral-tube GEP encapsulated with PCM, which increased heat exchange by 6.52 W/m, reduced surface temperature rise, and yielded a 3.38 % higher total HT than conventional GEPs. However, this configuration caused a slight increase in surface stress, initially up to 9.84 kPa, later stabilizing at 1.4 kPa.

As the complexity of GEP systems increased, research focus shifted toward understanding their thermomechanical behavior. Bao et al. [24] analyzed reinforced concrete GEPs embedded in saturated sandy soils under cyclic thermal loading. Their observations revealed non-uniform strain development, emphasizing the need to account for thermoplastic strain and soil consolidation in long-term structural design. Lou et al. [25] examined the behavior of pre-bored grouted planted (PGP) GEPs through two tests, one without and one with building load, demonstrating that thermally induced stress distributions were strongly affected by boundary restraints at the pile ends. Han et al. [26] developed a 3D model to investigate coupled thermo-hydro-mechanical responses under non-isothermal conditions. Their findings indicated that higher soil thermal conductivity and groundwater flow enhanced energy harvesting, although strong end-restraints reduced shaft resistance during thermal expansion. Moradshahi et al. [27] used numerical modeling to analyze stress and temperature gradients across pile cross-sections. They found that the central region experienced the highest stress concentrations, and noted that commonly used simplified models often result in overdesigns of up to 2 MPa. Du et al. [28] proposed an innovative GEP design incorporating hollow steel balls filled with PCM. Their simulations showed reduced temperature variations, strain, and displacement compared to conventional piles. Crucially, they highlighted the importance of aligning thermal loads with PCM melting temperatures for optimal performance.

Chang et al. [29] emphasized regional-scale energy planning by estimating the technical geothermal potential through a campus-based case study, illustrating the practical application of GEPs at localized scales. Complementing this, Baffa et al. [30] conducted a bibliometric and systematic review, identifying research trends and performance drivers in GEP applications for buildings. Time-dependent thermal behavior and pile group interactions were explored by Zhao et al. [31], while Fattahian et al. [32] investigated seasonal mixed convection effects, highlighting their role in energy efficiency under varying climatic conditions. Lupattelli and Salciarini [33] assessed thermal recovery in real-world foundations, showing how activation scenarios influence thermal sustainability. Song et al. [34] employed a load transfer method to analyze dissimilar pile group behaviors, revealing stress redistribution effects under thermal loads. Wang et al. [35] integrated explainable machine learning models to predict outlet temperatures, offering a data-driven approach to system control. Yuan et al. [36] and Erginag et al. [37] contributed experimental and numerical insights into buried GEP behavior and thermally induced tensile stresses, with direct implications for structural safety. Hu et al. [38] demonstrated the benefit of winter-mode energy injection to improve heat restoration, while Alqawasmeh et al. [39] emphasized the importance of accounting for hydrothermal spatial variability when designing pile groups. Theoretical modeling by Liu et al. [40] addressed thermo-hydro-mechanical behavior in partially saturated soils, and He et al. [41] quantified depth-dependent thermal loading responses. Zhuang et al. [42] examined non-uniform initial ground temperature distributions, contributing to more realistic thermo-mechanical simulations. Lastly, studies by Hu et al. [43] and Zhao et al. [44] investigated PCM-enhanced energy restoration cycles and the effects of lateral loading, respectively, enriching our understanding of GEP performance under both thermal and structural constraints.

Despite substantial progress in the field, existing experimental and numerical research on GEPs has primarily concentrated on enhancing thermal efficiency and optimizing general system performance. While various geometrical configurations have been explored, the majority of studies have focused on conventional or spiral designs, with limited attention given to the thermomechanical behavior of GEPs incorporating polygonal HE profiles such as square and triangular sections. Furthermore, most investigations are either thermally or mechanically focused, lacking a fully coupled three-dimensional thermomechanical analysis, particularly under realistic seasonal operating conditions.

To address these gaps, the present study conducts a comprehensive 3D numerical investigation into the coupled thermomechanical performance of GEP systems integrating U-shaped HEs with three different cross-sectional geometries: circular, square, and triangular. The study employs a robust finite volume-based numerical framework, incorporating a segregated solution strategy with under-relaxation techniques and the Pressure-Implicit with Splitting of Operators (PISO) scheme to ensure numerical stability and

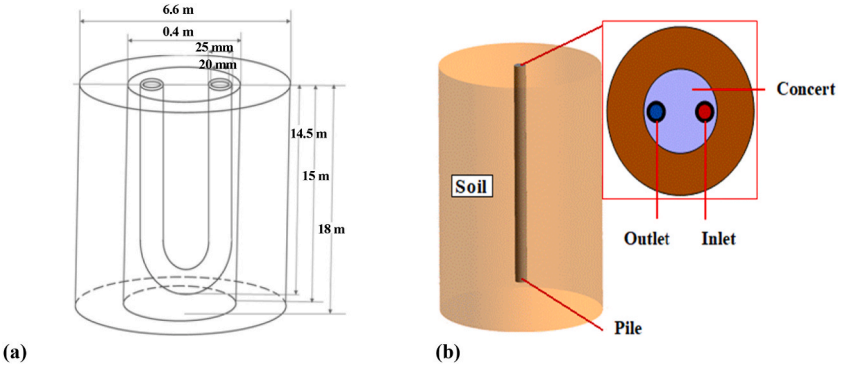


**Fig. 1.** HT model of GEP: (a) Schematic, (b) physical setup.

accuracy. Both spatial and temporal discretization are performed using second-order schemes to capture transient thermofluid and structural behavior under heating (summer) and cooling (winter) scenarios.

The objective of this research is to evaluate and compare the HT efficiency, temperature distribution, pile displacement, and stress responses of GEP systems with varying HE geometries. By analyzing these parameters under seasonal loading, the study aims to provide deeper insight into the influence of exchanger shape on overall system behavior, thereby supporting the design of more energy-efficient and structurally reliable GEP systems. Ultimately, the findings contribute to the development of high-performance, sustainable ground heat exchange technologies for renewable energy integration in buildings and infrastructure.

## 2. Theoretical modeling approach

### 2.1. Problem formulation

Fig. 1 presents the detailed geometric configuration of the proposed HT model designed to simulate the thermal behavior of a GEP system. The model is developed as a three-dimensional, axisymmetric representation of a typical energy pile embedded within a homogeneous soil mass. It incorporates four distinct but thermally and mechanically interactive domains: the soil matrix, the concrete pile, the embedded HE, and the circulating fluid. Each domain plays a critical role in the coupled thermomechanical response of the system.

The outermost domain comprises the surrounding soil, modeled as a vertical cylindrical volume with a diameter of 6.6 m and a depth of 18 m. This domain represents the thermal reservoir of the system, acting as both the heat sink and source depending on seasonal operating conditions. The soil's thermal and mechanical characteristics govern the rate of heat dissipation and the structural interaction with the pile.

Centrally located within the soil is the reinforced concrete pile, which serves dual purposes as both a load-bearing structural foundation and a medium for thermal exchange. The pile has a length of 15 m and a diameter of 0.4 m. Its material properties, especially thermal conductivity, heat capacity, and Young's modulus, are crucial to accurately capturing the thermal storage behavior and structural deformation under thermally induced stresses.

Embedded within the concrete pile is the U-shaped high-density polyethylene (HDPE) HE tube, forming the third domain of the model. This closed-loop tube extends to a depth of 14.5 m and is responsible for circulating the HT fluid, typically water, throughout the system. The internal and external diameters of the tube are 0.020 m and 0.025 m, respectively, which influence both fluid velocity and thermal boundary layer development. The tube's geometry and thermal resistance play a direct role in governing the efficiency of heat exchange between the fluid and the concrete pile.

The fourth domain is the fluid domain, comprising the water that circulates through the U-shaped HDPE tube. This domain is subject to internal convective HT mechanisms and is modeled using the appropriate thermophysical properties, including density, specific heat, viscosity, and thermal conductivity. The flow regime is assumed to be turbulent or laminar depending on the operating Reynolds number (Re), and it is driven by an imposed inlet velocity and outlet pressure, consistent with typical GEP operation.

To ensure geometric and physical accuracy, the dimensions and material properties employed in the current model are adapted from Zhang et al. [12], whose work provides a validated baseline for comparative studies. A detailed summary of the principal physical properties associated with each component is provided in Table 1.

This multi-domain configuration allows for a detailed and physically consistent representation of the energy pile's thermo-mechanical behavior, forming the foundation for subsequent numerical simulations aimed at evaluating the impact of HE geometry on system performance under various thermal loading conditions.

### 2.2. Mechanics model

To evaluate the mechanical response of the GEP system under vertical loading, a detailed mechanical model was developed, as illustrated in Fig. 2. The modeling approach follows the methodology outlined by Zhang et al. [12], with the objective of examining the distribution of displacements and stresses within the pile and the surrounding soil. This analysis helps to understand the load transfer mechanisms and the structural performance of the GEP under operational conditions.

A compressive load of 1,600,000 N was applied vertically to the top surface of the pile to simulate service conditions, such as building or infrastructure loads. The soil domain beneath the pile was assumed to be fully constrained, representing a rigid and immovable base, effectively imposing a fixed boundary condition. The lateral soil boundaries were restricted in the normal direction to prevent unrealistic lateral deformations. The interaction between the pile and the surrounding soil was modeled as a fully bonded

**Table 1**
Physical properties of materials used in the model.

| Material | Density (ρ) ($kg/m^3$) | Specific Heat ($C_p$) (j/kg.K) | Thermal Conductivity (λ) (W/m.K) |
|---|---|---|---|
| HDPE | 950 | 2300 | 0.44 |
| Concrete | 2300 | 850 | 1.54 |
| Clay soil | 2000 | 1644 | 1.877 |
| Water | 998.2 | 4182 | 0.6 |

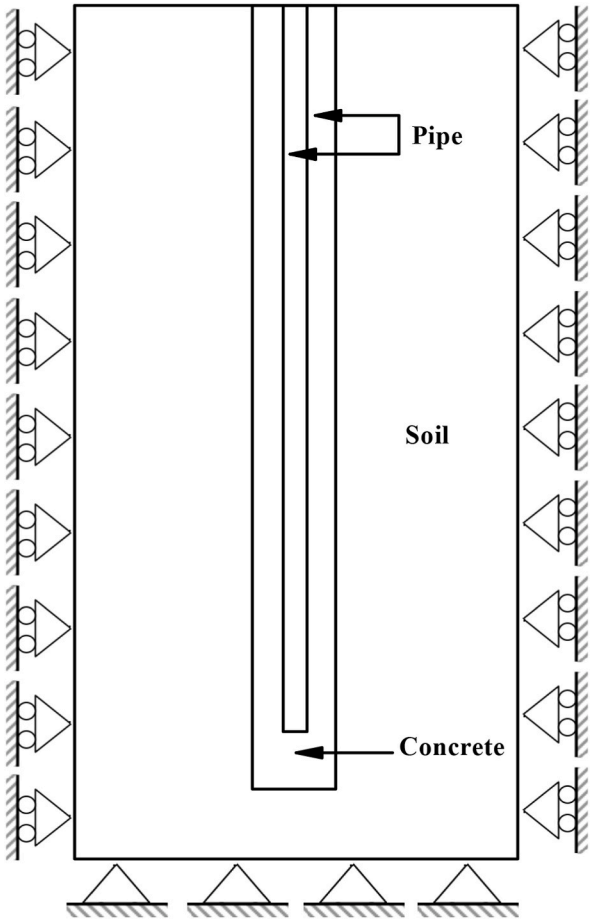


**Fig. 2.** Schematic representation of the mechanical model for the GEP system.

interface, incorporating both frictional resistance and normal contact pressure to realistically capture load transfer mechanisms.

The mechanical characteristics of the materials involved, including elastic modulus, Poisson's ratio, and other relevant parameters, are presented in Table 2. These values were sourced from Zhang et al. [12] and reflect the behavior of HDPE, concrete, and clay soil. Where applicable, thermal expansion coefficients are also included to support further investigations into coupled thermo-mechanical performance.

### *2.3. Analysis of the fundamentals of thermomechanical coupling*

This section outlines the key governing equations for HT and mechanical behavior under thermomechanical loading, based on Xu et al. [45].

#### *2.3.1. HT equations*

The study considers heat conduction in solids, governed by Fourier's law (Eq. (1)), and its transient form (Eq. (2)), which accounts for time-dependent temperature changes.

$$Q = -\lambda.\nabla T \tag{1}$$

**Table 2**
Mechanical properties of Materials used in the simulation.

| Material | Elastic moduls (GPa) | Poisson's ratio | Expansion angle (°) | Internal friction angle (°) | Thermal expansion coefficient ($°C^{-1}$) |
|---|---|---|---|---|---|
| HDPE | 1.1 | 0.42 | – | – | 0.00023 |
| Concrete | 30 | 0.20 | – | – | $10^{-5}$ |
| Clay soil | 0.015 | 0.33 | 0 | 31 | – |

$$\rho_s C_{ps}\left(\frac{\partial T}{\partial t}+u_{trans}\nabla T\right)+\nabla(q+q_r)=Q \tag{2}$$

In fluids, convective HT is described by an energy conservation equation (Eq. (3)), which simplifies under low-compressibility conditions (e.g., water) to omit pressure work (Eq. (4)).

$$\rho_f C_{pf}\left(\frac{\partial T}{\partial t}+u\nabla T\right)+\nabla(q+q_r)=\alpha_f T\left(\frac{\partial p}{\partial t}+u\nabla p\right)+\tau:\nabla u+Q \tag{3}$$

$$\rho_f C_{pf}\frac{\partial T}{\partial t}+\rho_f C_{pf}\,u\nabla T+\nabla(-\lambda\nabla T)=Q \tag{4}$$

### 2.3.2. Mechanical equations

Axial displacement in piles is analyzed under mechanical loading (Eq. (5)) and thermal expansion (Eq. (6)), with their combined effect given by Eq. (7).

$$\delta_{mech}=\frac{FL}{EA} \tag{5}$$

$$\delta_{T,i}=\delta_{T,i-1}+\frac{1}{2}\left(\epsilon_{T,i-1}+\epsilon_{T,i}\right)\Delta l \tag{6}$$

$$\delta_{Total,i}=\delta_{mech}+\delta_{T,i} \tag{7}$$

Free thermal strain (Eq. (8)) represents unconstrained expansion, while thermal stress (Eq. (9)) and axial force (Eq. (10)) arise when expansion is restrained.

$$\epsilon_{T-free}=\alpha.\Delta T \tag{8}$$

$$\sigma=E.\epsilon_{T-free}=E\,\alpha\,\Delta T \tag{9}$$

$$F=\sigma.A=E.\alpha.\Delta T.A \tag{10}$$

The residual strain due to soil confinement (Eq. (11)) and the resulting modified axial stress (Eq. (12)) reflect the influence of pile–soil interaction on thermally induced stresses.

$$\epsilon_{res}=\epsilon_{T-free}-\epsilon_T \tag{11}$$

$$\sigma_{res}=E\,\epsilon_{res}=E\left(\epsilon_{T-free}-\epsilon_T\right)=E(\alpha.\Delta T-\epsilon_T) \tag{12}$$

## 3. Numerical modeling

### 3.1. Turbulence model

In GEP systems, the high Re numbers typically encountered result in turbulent flow, necessitating a reliable turbulence model to accurately capture the interactions between velocity, pressure, and temperature fields. For this purpose, the standard $k$-$\varepsilon$ turbulence model [46] was selected due to its robustness and computational efficiency in engineering applications.

Simulations were conducted using ANSYS Fluent 20.0, which solves the coupled mass, momentum, and energy equations under turbulent flow conditions. The governing equations include [46,47]:

(i) Continuity equation:

$$\frac{\partial\rho}{\partial t}+\frac{\partial U_i}{\partial X_i}=0 \tag{13}$$

(ii) Momentum equation:

$$U_j\frac{\partial U_i}{\partial X_j}=-\frac{1}{\rho}\frac{\partial P}{\partial X_i}+\vartheta\frac{\partial^2 U_i}{\partial X_j\partial X_j} \tag{14}$$

(iii) Energy equation:

$$U_j\frac{\partial T}{\partial X_j}=\frac{1}{\rho}\frac{\partial P}{C_p}\left(\frac{\lambda\partial^2 T}{\partial x_j\partial x_j}+\phi\right) \tag{15}$$

(iv) Turbulent kinetic energy ($k$) equation:

$$\rho\left(\frac{\partial k}{\partial t}+U_j\frac{\partial k}{\partial X_j}\right)=\frac{\partial}{\partial X_j}\left[\left(\mu+\frac{\mu_t}{\sigma_k}\right)\frac{\partial k}{\partial X_j}\right]+G_k-\rho\varepsilon \tag{16}$$

(v) Turbulence dissipation rate ($\varepsilon$) equation:

$$\rho\left(\frac{\partial \varepsilon}{\partial t}+U_j\frac{\partial \varepsilon}{\partial X_j}\right)=\frac{\partial}{\partial X_j}\left[\left(\mu+\frac{\mu_t}{\sigma_\varepsilon}\right)\frac{\partial \varepsilon}{\partial X_j}\right]+C_{\varepsilon 1}\frac{\varepsilon}{k}G_k-C_{\varepsilon 2}\rho\frac{\varepsilon^2}{k} \tag{17}$$

The turbulent viscosity ($\mu_t$) is calculated using:

$$\mu_t=C_\mu\,\rho\frac{k^2}{\varepsilon} \tag{18}$$

The system is completed by standard model constants associated with the $k$-$\varepsilon$ formulation, as listed in Eq. (20):

$$C_\mu=0.09, C_{\varepsilon 1}=1.44, C_{\varepsilon 2}=1.92, \sigma_k=1.0, \text{and } \sigma_\varepsilon=1.3 \tag{20}$$

This set of equations forms a closed system for simulating turbulent flows with heat transfer, allowing for accurate resolution of the thermal-hydraulic behavior in GEP systems.

### 3.2. Initial and boundary conditions

The reliability and accuracy of the computational simulations conducted in this study depend critically on the appropriate definition of both initial conditions and boundary conditions across the fluid and soil domains, with particular attention to mechanical and thermal interactions under seasonal loading conditions. The modeled system consists of a U-shaped ground HE embedded in a soil medium, where HT and fluid flow are coupled with mechanical interactions between the geothermal pile and surrounding soil.

To ensure physical realism, mechanical boundary conditions were imposed in accordance with actual in-situ behavior, reflecting how the pile transmits axial loads through the soil medium. These were defined based on established procedures referenced in Zhang et al. [12].

#### 3.2.1. Mechanical boundary conditions

*3.2.1.1. Pile–soil interface.* The contact between the pile and soil was modeled as a fully bonded interface, assuming no slippage under load. This condition simulates either perfect adhesion or sufficient frictional resistance at the interface to prevent tangential displacement. Both normal and tangential stresses were transmitted through the interface, allowing for a realistic simulation of load transfer via shaft resistance along the embedded length of the pile.

*3.2.1.2. Pile head boundary condition.* To simulate the mechanical response of the pile under vertical loading, a static axial force of 1600 kN was applied to the top of the pile. The head of the pile was modeled as restrained in lateral directions and rotation, while permitting vertical movement under the applied load. This boundary condition replicates field conditions where the pile head is not fully fixed but is constrained against horizontal displacement and rotation by the pile cap or superstructure. The adopted model allows vertical settlement to occur, enabling accurate stress distribution modeling and displacement feedback under axial load.

*3.2.1.3. Pile base boundary condition.* At the base, the pile was assumed to be in full contact with the surrounding soil, enabling the transfer of vertical stresses through end-bearing action. However, no artificial fixity was imposed; instead, the base was free to settle under the applied load. This approach avoids over-constraining the model and allows the soil–pile interaction to determine the extent of base resistance through normal contact pressures and passive bearing mechanisms.

These boundary conditions collectively facilitate a realistic simulation of axial load transmission from the pile head through both shaft resistance and end-bearing mechanisms, enabling the accurate prediction of settlement, stress distribution, and pile–soil mechanical response under operational conditions.

#### 3.2.2. Fluid domain boundary conditions

To simulate HT and fluid flow (FF) phenomena within the U-shaped ground HE, consistent velocity and temperature boundary conditions were specified at the inlet of the flow domain. The fluid velocity was maintained at a constant value of 0.6 m/s, ensuring a uniform and stable internal flow regime across both seasonal scenarios.

In the winter simulation, the fluid enters the domain at a temperature of 278.15 K, reflecting typical cold-season operation, where the fluid gains heat from the warmer soil. In contrast, during the summer simulation, the inlet temperature was set at 318.15 K, representing a cooling mode where the fluid releases heat to the surrounding soil. The outlet boundary was treated as a pressure outlet, allowing fluid to exit naturally without artificially constraining the thermal or flow profile. Table 3 summarizes the boundary condition parameters for the winter scenario, while Table 4 presents those for the summer simulation.

#### 3.2.3. Soil domain boundary conditions

The surrounding soil was modeled as a thermally active but mechanically passive medium, with a fixed temperature boundary condition of 291.89 K applied uniformly. This value represents an average deep ground temperature assumed to remain constant throughout the relatively short simulation period. The initial temperature across the soil domain was set to the same value. No external mechanical constraints were imposed on the soil boundaries, allowing for natural development of stress fields due to the combined effects of axial loading and thermal interactions with the pile.

### 3.3. Numerical procedure

The numerical procedure employs ANSYS Fluent 20.0 to simulate FF and HT dynamics using a 3D segregated, pressure-based Navier-Stokes solver with double precision. The finite volume method (FVM) [48] is applied implicitly, and the PISO algorithm handles pressure-velocity coupling. Governing equations are discretized using the second-order upwind (SOU) scheme and a bounded second-order implicit method for transient calculations. Simulations run over 48-h intervals to capture FF evolution with stability and accuracy.

### 3.4. Mesh sensitivity test

To ensure the accuracy and reliability of the numerical simulations, a comprehensive mesh sensitivity analysis was performed. Five distinct grid configurations with progressively refined element sizes were generated to evaluate the influence of mesh density on the solution's stability and precision. Due to the geometric complexity of the GEP system, an unstructured mesh approach was adopted, employing tetrahedral elements for general domain coverage and prism layers near solid boundaries to resolve near-wall gradients more effectively. This configuration was particularly suitable for capturing the intricate flow and thermal interactions within the system.

Enhanced wall treatment functions were employed in the simulations to ensure accurate modeling of the near-wall region. A targeted dimensionless wall distance ($y^+$) of approximately 1 was maintained to resolve the viscous sublayer and accurately capture wall HT and wall shear stress. This fine near-wall resolution was essential for preserving the fidelity of the thermal and hydrodynamic predictions.

The convergence behavior and accuracy of the simulation results were rigorously examined across all five grid levels, with detailed outcomes summarized in Table 5. Based on residual stability and key output parameters, Grid (4) emerged as the optimal configuration, offering a balance between computational efficiency and numerical accuracy. This grid was subsequently converted into a polyhedral mesh to further enhance numerical robustness and reduce solution time.

Upon re-running the simulation with the polyhedral mesh, the results, presented in Table 6, demonstrated increased precision and a marked reduction in computational time, as illustrated in Fig. 3. Importantly, attempts to further refine the mesh beyond this level showed marginal improvements in accuracy, while significantly escalating computational demands. This confirmed that Grid (4), in its polyhedral form, provided a grid-independent solution, making it the preferred choice for the final simulation analysis.

### 3.5. Model verification and validation

To verify the reliability and precision of the computational approach used in this research, it is essential to validate the findings by comparing them with data from previous studies conducted under similar conditions. The current evaluation of the GEP system is compared with both numerical and field test results from a project in Kunshan, Jiangsu Province, as reported by Zhang et al. [12]. In this validation process, the geometric parameters and material properties of the pipes, concrete, soil, fluids, and boundary conditions from the referenced study were replicated to assess the thermal and mechanical behaviors, as well as the thermo-mechanical coupling interactions, in the present model.

In the referenced study, the GEP system is 15 m long and 0.4 m in diameter, constructed from concrete. The surrounding soil is clay, extending to a diameter of 0.6 m and a length of 18 m. The HE is made of polyethylene and configured as a double U-shaped pipe with a diameter of 0.025 m, whereas the present study employs a single U-shaped pipe. During winter, the inlet fluid temperature is 278.15 K, while in summer it is 318.15 K. The soil temperature remains constant at 291.89 K for both heating and cooling purposes, and a mechanical load of 1,600,000 N is applied to the pile. The findings are summarized in Tables 7 and 8.

Table 7 shows that under winter conditions, the increase in outlet water temperature ($T_{outlet}$) in Zhang et al.'s study [12] was 1.20 K in the experimental case and 1.28 K in the numerical case. In the present study, the simulated increase was 1.03 K, while the analytical increase was 1.75 K. This results in discrepancies of 0.25 K and 0.17 K for the numerical values, and 0.47 K and 0.55 K for the analytical values, compared to Zhang et al.'s experimental and numerical results [12], respectively.

**Table 3**
Boundary condition parameters for winter simulation of the computational domain.

| Boundary | Boundary condition | Value | Mode |
|---|---|---|---|
| Inlet | Velocity inlet | 0.6 [m/s] | Heating |
| | Temperature inlet | 278.15 [K] | |
| Domain soil | Temperature | 291.89 [K] | |

**Table 4**
Thermal and flow boundary conditions for summer period simulation.

| Boundary | Boundary condition | Value | Mode |
|---|---|---|---|
| Inlet | Velocity inlet | 0.6 [m/s] | Cooling |
| | Temperature inlet | 318.15 [K] | |
| Domain soil | Temperature | 291.89 [K] | |

**Table 5**
Mesh sensitivity analysis with associated computational time.

| | Grid (1) | Grid (2) | Grid (3) | Grid (4) | Grid (5) |
|---|---|---|---|---|---|
| Cells | 2702898 | 3198148 | 5730595 | 8859429 | 13480156 |
| $T_{inlet}$ [K] | 318.15 | 318.15 | 318.15 | 318.15 | 318.15 |
| $T_{outlet}$ [K] | 316.215 1.935 | 316.149 | 316.141 | 316.132 | 316.131 |
| $\Delta T$ [K] | 1.935 | 2.001 | 2.009 | 2.018 | 2.019 |
| Computing time | 00h 46min | 01h 17min | 02h 20min | 03h 50min | 05 h05min |

**Table 6**
Computational comparison between unstructured and polyhedral meshes.

| Mesh (4) | | |
|---|---|---|
| Type | Unstructured | Polyhedral |
| Number of elements | 8859429 | 3198148 |
| $T_{inlet}$ [K] | 318.15 | 318.15 |
| $T_{outlet}$ [K] | 316.132 | 316.128 |
| $\Delta T$ [K] | 2.018 | 2.022 |

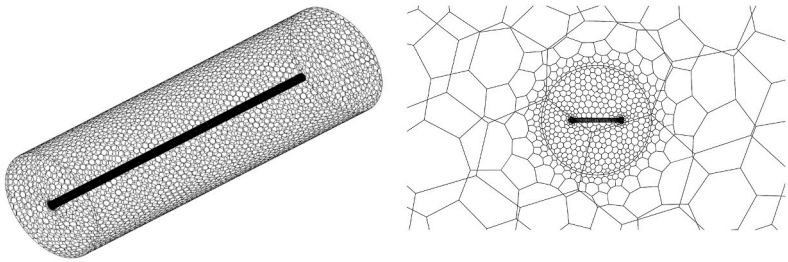

**(a)** **(b)**

**Fig. 3.** Mesh study results: (a) Three-dimensional view of the polyhedral mesh, (b) Two-dimensional cross-section of the polyhedral mesh.

**Table 7**
Comparison of simulated and measured outlet water temperatures.

| Authors | Pipe Configuration | Pile Size (m) | Software | Periods | $T_{inlet}$ (K) | $T_{outlet}$ (K) | Study | $t$ (hours) | $\Delta T$ (K) |
|---|---|---|---|---|---|---|---|---|---|
| Zhang et al. [12] | Double U-shaped | Diameter = 0.4 | ANSYS Workbench | Summer | 318.15 | 315.35 | Numerical | 36 | 2.80 |
| | | | | Winter | 278.15 | 279.43 | | | 1.28 |
| | | Length = 15 | | Summer | 318.15 | 314.66 | Tester | | 3.49 |
| | | | | Winter | 278.15 | 279.38 | | | 1.20 |
| Present study | U-shaped | Diameter = 0.4 | ANSYS Fluent 20.0 | Summer | 318.15 | 316.12 | Numerical | 48 | 2.03 |
| | | | | Winter | 278.15 | 279.18 | | | 1.03 |
| | | Length = 15 | | Summer | 318.15 | 314.81 | Analytical | 48 | 3.34 |
| | | | | Winter | 278.15 | 279.90 | | | 1.75 |

Under summer conditions, the decrease in $T_{outlet}$ in Zhang et al.'s study [12] was 3.49 K in the experimental case and 2.80 K in the numerical case. In contrast, the present study reported a decrease of 2.03 K for the numerical values and 3.43 K for the analytical values. The differences in temperature decrease are 1.46 K and 0.77 K for the numerical values, and 0.15 K and 0.54 K for the analytical values, compared to Zhang et al.'s results [12].

Table 8 presents the shrinkage and expansion of the pile under winter and summer conditions. During winter, Zhang et al. [12]

**Table 8**
Displacement response comparison across various scenarios.

| Authors | Pipe Configuration | Pile Size (m) | Software | Condition | Study | Displacement (mm) | Compressive stress (MPa) |
|---|---|---|---|---|---|---|---|
| Zhang et al. [12] | Double U-shaped | Diameter = 0.4<br>Length = 15 | ANSYS Workbench | - Pure mechanical load<br>- Thermal coupling at winter<br>- Thermal coupling at summer<br>- Pure mechanical load<br>- Thermal coupling at winter<br>- Thermal coupling at summer | Numerical<br><br><br>Tester<br><br> | 2.45<br>3.24<br>2.41<br>2.35<br>3.47<br>2.18 | 3.183<br>0.600<br>0.650<br>/<br>/<br>/ |
| Present study | U-shaped | Diameter = 0.4<br>Length = 15 | ANSYS Fluent 20.0 | - Pure mechanical load<br>- Thermal coupling at winter<br>- Thermal coupling at summer | Numerical | 1.76<br>1.67<br>1.75 | 1.5894<br>1.5453<br>1.5107 |

reported a shrinkage of 1.12 mm in the experimental case and 0.79 mm in the numerical case. In the present study, the numerical shrinkage was 0.09 mm. Under summer conditions, the pile exhibited expansion. Zhang et al. [12] observed an elongation of 0.17 mm in the experimental case and 0.04 mm in the numerical case, while the present study recorded a slight elongation of 0.01 mm.

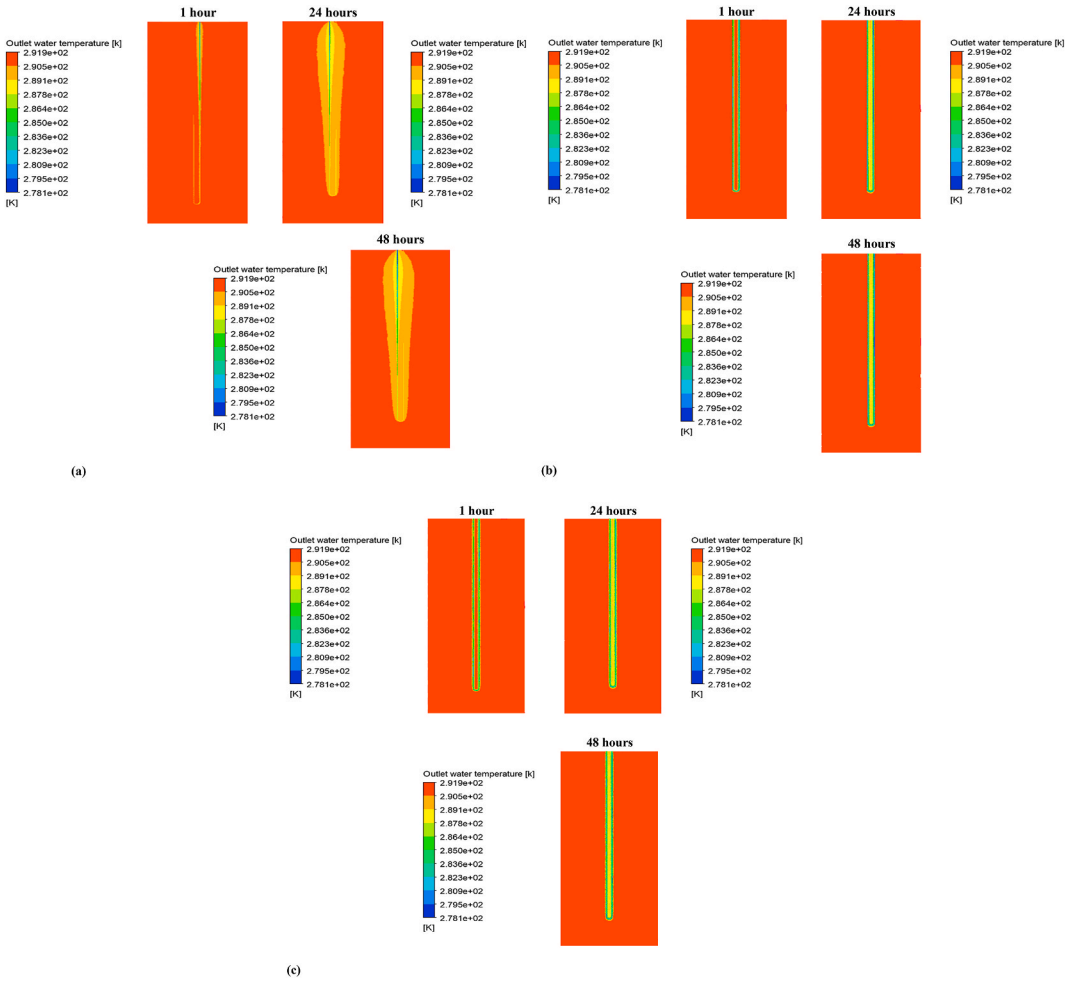


**Fig. 4.** Longitudinal temperature profiles in U-tube GEP Systems with (a) Circular, (b) Triangular, and (c) Square cross-sections during winter operation.

Under thermo-mechanical coupling effects during summer conditions, the circular configuration exhibited the highest axial compressive stress in the present study, with an increase of approximately 0.0787 MPa. Conversely, in winter conditions, the stress decreased by about 0.0441 MPa. In comparison, the numerical results reported by Zhang et al. [12] indicated a significantly greater variation, with the maximum axial compressive stress rising by approximately 2.533 MPa in summer and declining by around 2.583 MPa in winter.

The discrepancies observed in the results can be attributed to several contributing factors, including variations in HE designs, differences mechanical conditions, differences in mesh sensitivity, and the influence of groundwater dynamics. Seasonal fluctuations in soil temperature also play a critical role, particularly given the heterogeneous nature of the unstructured soil formation, which comprises multiple layers with distinct thermal and mechanical properties. Among these, thermal conductivity significantly affects the thermal response and overall performance of GEP. Furthermore, computational variations arising from the use of different hardware configurations and versions of ANSYS software may also introduce slight differences in simulation outcomes. Despite these factors, the strong agreement between the numerical and analytical predictions for outlet water temperature and HE performance in the present study reinforces the credibility and reliability of the modeling approach.

## 4. Analysis of results and comprehensive discussion

### 4.1. Thermal performance assessment

The temporal evolution of the thermal distribution within GEP systems utilizing U-tube HE configurations of circular, triangular, and square cross-sectional geometries is illustrated in Figs. 4 and 5, specifically under winter operating conditions. These figures provide detailed representations of both longitudinal and transverse temperature profiles at three distinct time intervals: 1 h, 24 h, and 48 h.

In the initial hour of system operation, all configurations exhibited a pronounced and abrupt decline in fluid temperature, reflecting an immediate and intensive heat extraction from the surrounding soil. This initial thermal response is indicative of a strong thermal

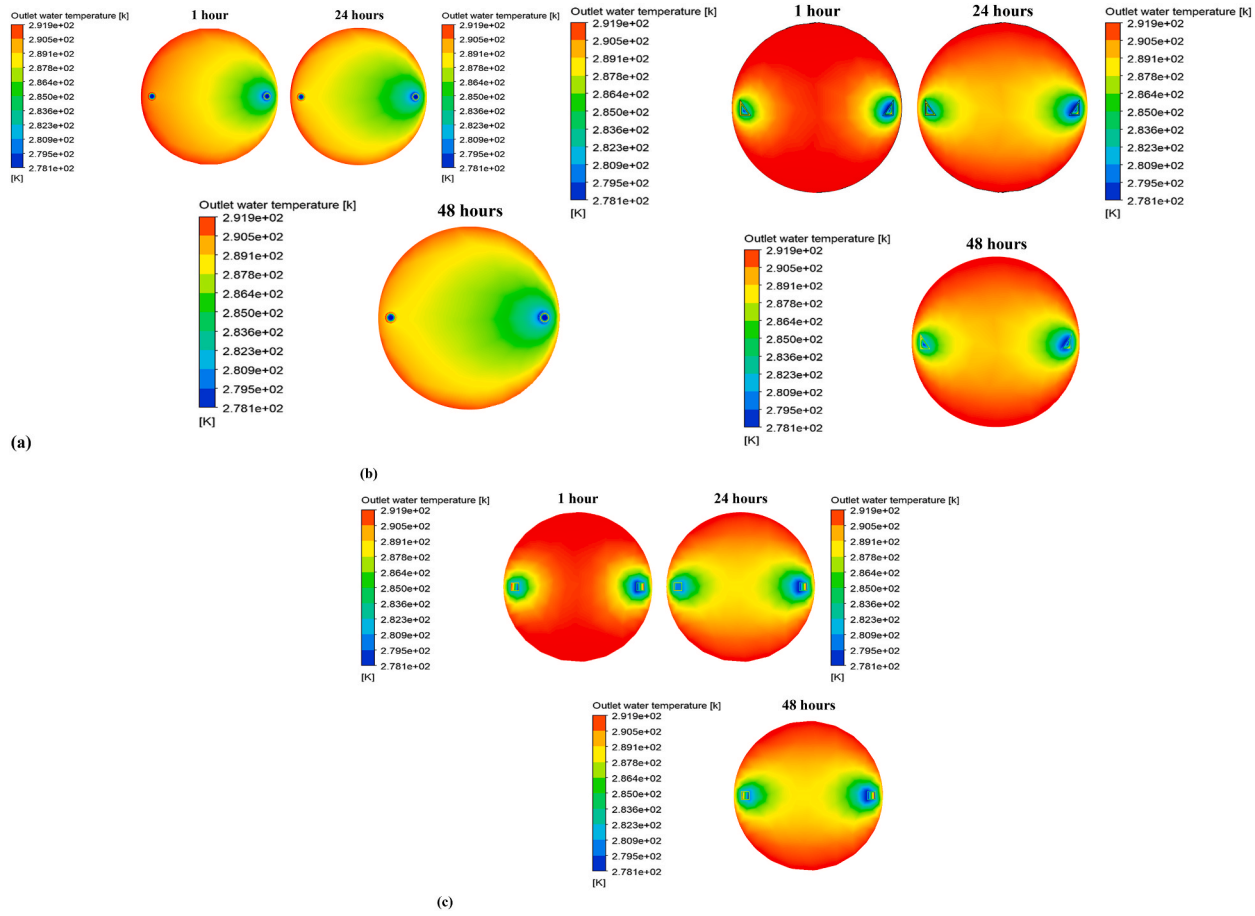


**Fig. 5.** Transverse temperature distribution in GEP systems with (a) circular, (b) triangular, and (c) square U-tube configurations under winter operating conditions.

gradient between the circulating fluid and the relatively undisturbed ground, facilitating rapid HT.

As the operational period extended to 24 h, this cooling trend persisted and even intensified, highlighting a continued and efficient HT process. The ongoing decline in temperature suggests that the thermal energy of the soil was still actively being drawn into the fluid, supported by the sustained thermal gradient.

However, by the 48-h mark, the temperature drop across all geometries became minimal, indicating a reduced thermal gradient and diminished heat exchange performance, likely due to thermal saturation of the surrounding soil.

In contrast to winter-mode operation, Figs. 6 and 7 illustrate the temperature contours for the same GEP configurations, circular, triangular, and square U-tube cross-sections, under summer-mode conditions. During the initial hour of operation, a clear and measurable increase in soil temperature was observed surrounding all GEP types, signifying the commencement of heat injection from the working fluid into the ground. This early thermal response highlights the strong initial thermal gradient between the relatively cooler subsurface and the warmer circulating fluid, which facilitates rapid HT into the surrounding soil.

As the operation progressed to the 24-h mark, the thermal contours showed a continued and substantial rise in temperature within the soil adjacent to the GEPs. This trend indicates sustained HT and strong thermal interaction between the U-tube systems and the surrounding ground, with thermal energy diffusing outward from the pipe surfaces into the soil matrix.

However, by 48 h of continuous operation, the rate of temperature increase had markedly decreased across all configurations, and the contours began to stabilize. This plateau in temperature distribution suggests that the surrounding soil had undergone significant

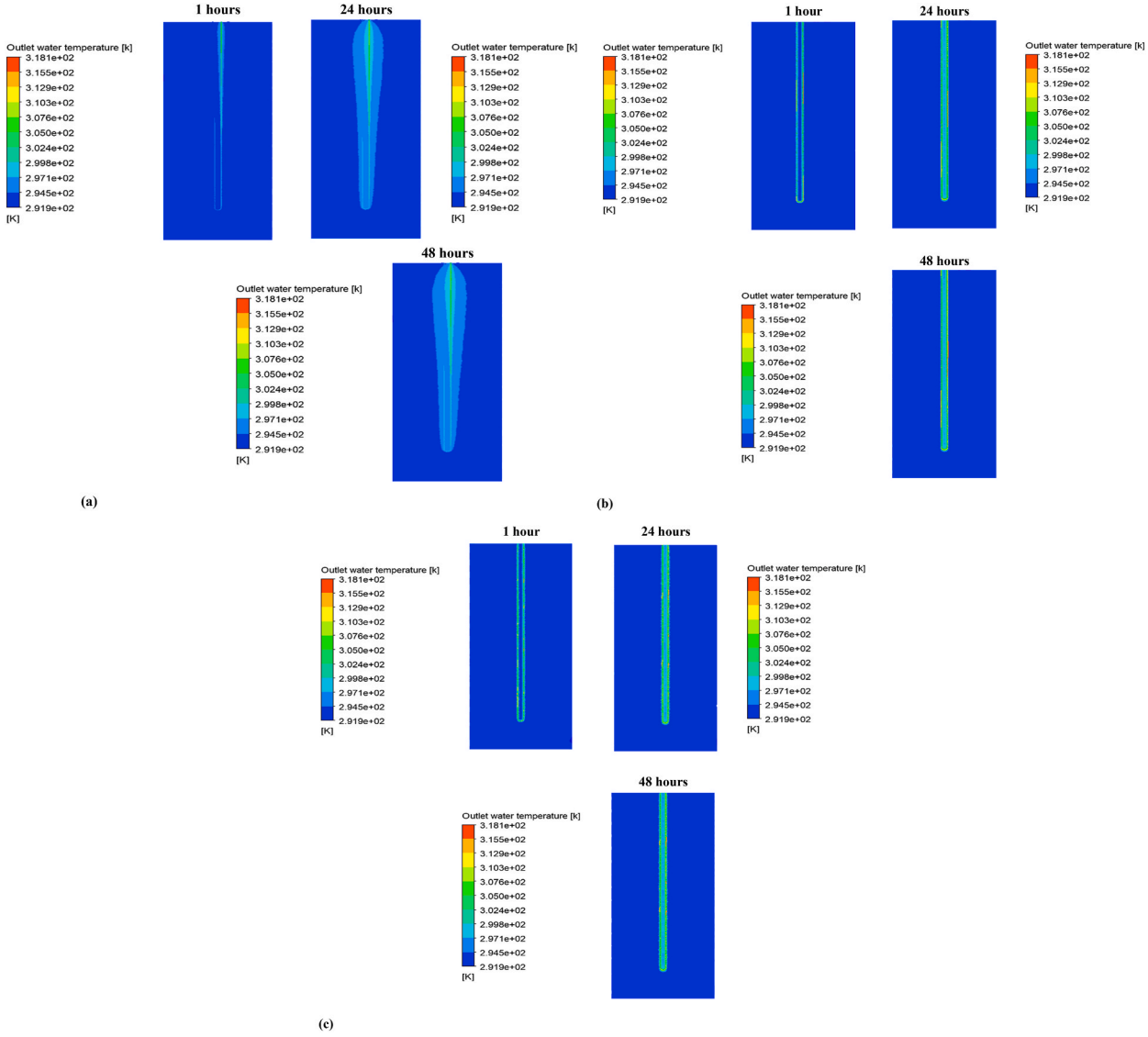


**Fig. 6.** Longitudinal temperature field distribution in GEP Systems with (a) Circular, (b) Triangular, and (c) Square U-tube configurations under summer operating conditions.

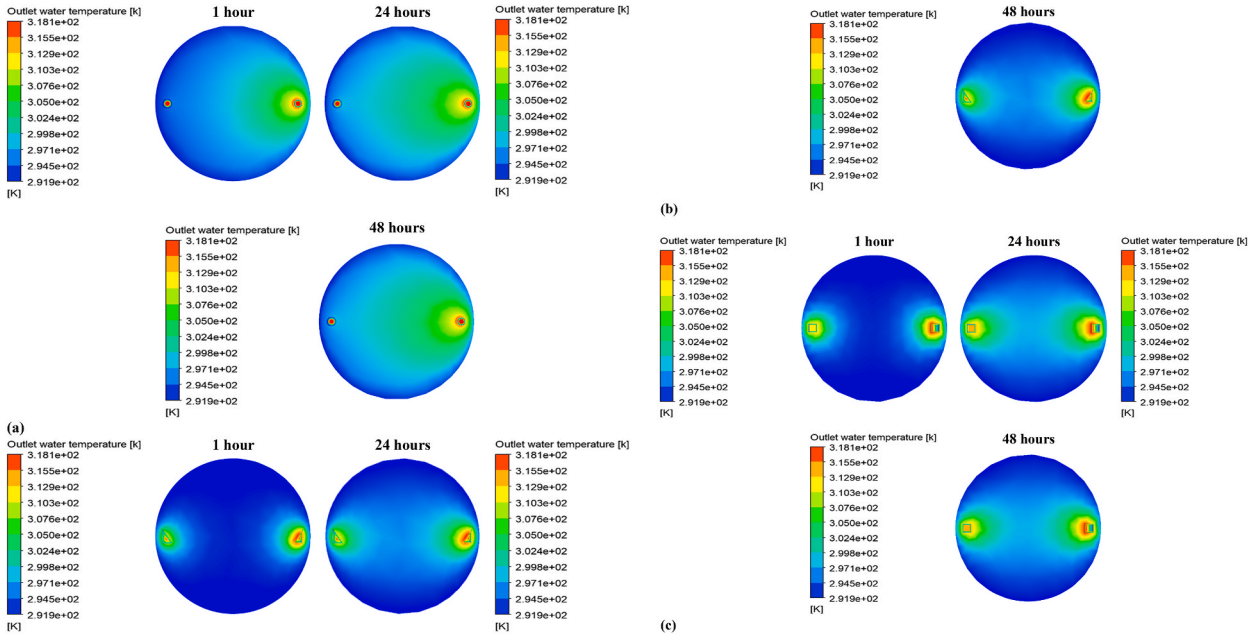


**Fig. 7.** Transverse temperature distribution patterns in GEP Systems with (a) Circular, (b) Triangular, and (c) Square U-tube configurations under summer operating conditions.

thermal accumulation, leading to a reduced thermal gradient between the U-tube fluid and the ground. Consequently, the rate of HT diminished, indicating a transition toward thermal equilibrium.

The thermal response of buried heat exchanger systems evolves through distinct operational phases, marked initially by a rapid heat transfer period followed by gradual thermal stabilization during both summer and winter seasons. At the onset of operation, all pipe geometries exhibit a sharp temperature shift, primarily driven by the pronounced thermal gradient between the circulating fluid and the undisturbed surrounding soil. This steep gradient promotes efficient heat transfer via both conduction and convection mechanisms. However, this phase is transient in nature and diminishes progressively as the system approaches thermal equilibrium.

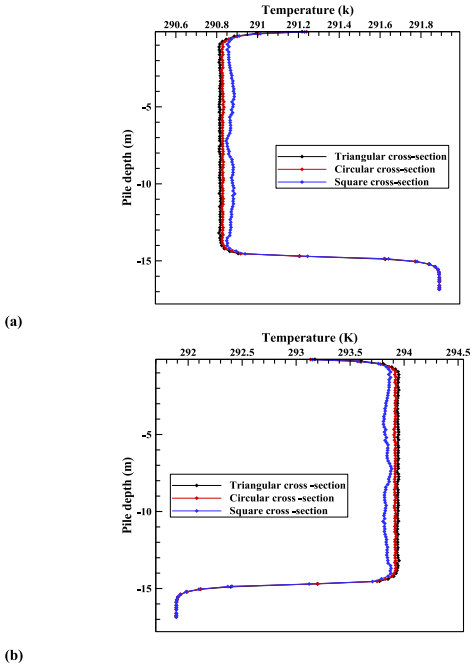


**Fig. 8.** Vertical temperature profiles along GEP depth with (a) Heating and (b) Cooling modes for different U-tube geometries.

After approximately 48 h of continuous operation, temperature profiles begin to stabilize, signaling the formation of a thermal boundary layer around the pipe. In this stabilized phase, the surrounding soil becomes increasingly saturated with heat under cooling conditions, or thermally depleted during heating, which in turn reduces the local temperature gradient and diminishes the driving force for continued heat exchange. This behavior is characteristic of buried heat exchanger systems and underscores the importance of implementing rest intervals or staggered operational strategies to minimize thermal fatigue and enhance long-term energy exchange efficiency.

The thermal behavior of U-shaped GEPs equipped with varying U-tube geometries, circular, triangular, and square, was thoroughly examined through vertical soil temperature profiling. The resulting distributions along the depth of the pile, under both heating (winter) and cooling (summer) modes, are depicted in Fig. 8(a) and (b), respectively.

In winter operation, as shown in Fig. 8(a), a distinct vertical temperature gradient is observed within the upper 1.5 m of the soil, where a steep temperature drop occurs due to intensive heat extraction by the circulating fluid. This indicates a strong thermal interaction between the GEP and the surrounding ground near the surface, driven by the initially high thermal gradient. Beyond this zone, from approximately 1.5 m–15 m depth, the temperature decline becomes more gradual yet continuous, reflecting a sustained but less intense HT process as the gradient decreases with depth. Notably, between 15 m and 16 m, the region devoid of embedded U-tube elements, the thermal profile begins to stabilize, forming a plateau that indicates minimal heat exchange activity due to the absence of direct thermal interaction with the system. This overall behavior remains consistent across all pipe geometries, signifying a shared trend in downward heat extraction performance.

Conversely, the summer-mode results shown in Fig. 8(b) exhibit an inverted trend, with a sharp rise in soil temperature within the top 1.5 m, corresponding to the initial zone of active heat injection. This upward temperature trend persists, with slight fluctuations, throughout the 1.5 m–15 m depth range, illustrating continued heat rejection into the surrounding ground. Similar to the winter case, the 15 m–16 m segment displays a nearly flat thermal profile, stabilizing at approximately 291.89 K, which again corresponds to the section without thermal influence from the U-tubes.

When evaluating the thermal responses across the three U-tube geometries, the circular and triangular configurations exhibit nearly overlapping temperature distributions along the entire depth. This similarity suggests comparable thermal performance in both heating and cooling scenarios. In contrast, the square U-tube configuration displays a noticeably different behavior. During the winter cycle, it produces a higher soil temperature profile, indicating less effective heat extraction and, therefore, lower heating efficiency. In the summer cycle, it results in a relatively lower soil temperature profile, which implies reduced heat rejection capability and sub-optimal cooling performance.

Soil heat absorption and the influence of pipe geometry on thermal propagation are critical factors affecting the performance of buried heat exchanger systems. The surrounding soil functions as a thermal buffer, facilitating the absorption and diffusion of heat during system operation. In both summer and winter conditions, heat transfer into the soil occurs predominantly through conduction. Temperature distribution analyses reveal that triangular pipe geometries promote more rapid and extensive lateral heat propagation compared to other configurations. This enhanced performance is likely attributable to the sharper external angles of the triangular

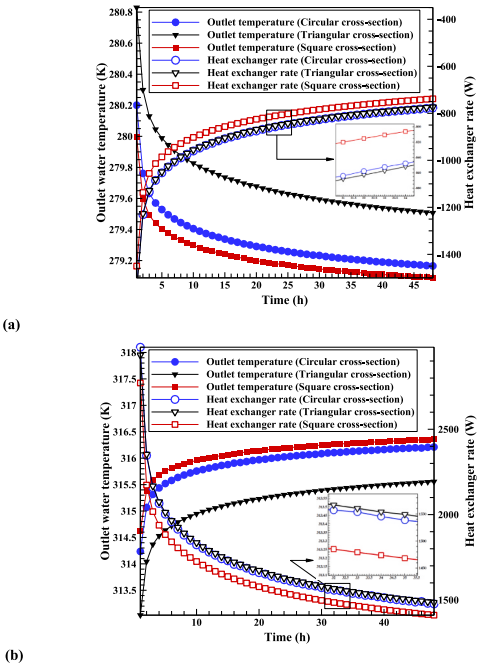


**Fig. 9.** Effect of U-tube cross-section geometry on water $T_{outlet}$ and heat exchange rate in GEP Systems during (a) Heating and (b) Cooling modes.

cross-section, which intensify thermal flux concentration into the adjacent soil. In contrast, square pipe geometries exhibit slower and less uniform thermal dispersion, likely due to geometric constraints and flow channeling effects that limit heat diffusion across the soil matrix. These findings underscore the significant impact of pipe geometry on soil thermal behavior and highlight its importance in optimizing the design and long-term efficiency of buried heat exchanger systems.

Fig. 9 presents a comparative analysis of the temporal evolution of the water $T_{outlet}$ and heat exchange rate for GEP systems equipped with circular, triangular, and square U-tube geometries. All configurations maintain identical foundation properties and geometrical dimensions, ensuring that performance differences are solely attributable to pipe geometry. The results encompass both heating (winter) and cooling (summer) operating modes, providing insights into the dynamic thermal behavior of each design over time.

During the winter heating mode, illustrated in Fig. 9(a), the triangular pipe configuration consistently exhibits a slight but measurable thermal advantage in terms of water $T_{outlet}$. Specifically, the $T_{outlet}$ for the triangular geometry is approximately 0.34 K higher than that of the circular configuration and 0.42 K higher than the square counterpart. This indicates less effective heat extraction from the ground, as the higher $T_{outlet}$ reflects reduced thermal energy gain by the fluid. Interestingly, this thermal behavior is accompanied by a lower heat exchange rate, by about 3.96 W compared to the circular pipe and 38.93 W relative to the square pipe. Despite the elevated $T_{outlet}$, the reduced HT rate suggests limited thermal interaction with the surrounding soil. This phenomenon can be attributed to the triangular tube's geometry, which provides a relatively smaller and non-uniform contact area with the soil, thereby constraining conductive HT. Additionally, the angular geometry may induce irregular boundary layer development along the external surface of the pipe, which can hinder effective heat dissipation into the surrounding soil. In contrast, the circular pipe provides a more uniform flow path that supports stable and symmetric convective flow around its perimeter. However, due to the absence of sharp edges or features that promote internal turbulence, it exhibits slightly lower thermal performance compared to the triangular configuration, which benefits from enhanced mixing and localized heat transfer intensification.

Conversely, under summer cooling conditions as illustrated in Fig. 9(b), the triangular configuration demonstrates markedly superior thermal performance. The water $T_{outlet}$ for the triangular tube is approximately 0.65 K lower than that of the circular tube and 0.80 K lower than the square configuration, indicating more effective heat extraction from the circulating fluid to the surrounding soil. Concurrently, the triangular configuration achieves the highest heat exchange rate, exceeding those of the circular and square designs by approximately 8.61 W and 74.41 W, respectively. This substantial improvement is primarily attributed to enhanced internal convective HT dynamics. The sharp corners and angular flow paths characteristic of the triangular geometry promote localized turbulence and secondary flow structures, even at moderate Re numbers, thereby increasing the convective HT coefficient along the inner surface. As a result, the triangular pipe enables more efficient thermal rejection to the ground, yielding both a lower $T_{outlet}$ and a higher heat transfer rate. In contrast, the square geometry, despite its higher perimeter-to-area ratio, suffers from adverse flow phenomena such as corner-induced recirculation zones and stagnation regions, which limit convective HT effectiveness and degrade overall thermal performance. The circular configuration offers a more stable and uniform flow path, supporting consistent convective behavior; however, it lacks geometrical features that enhance turbulence, resulting in moderately lower convective efficiency compared to the triangular design. Collectively, these results underscore the superior heat rejection capability of the triangular geometry in summer operating conditions, as evidenced by its reduced outlet temperature and significantly enhanced thermal exchange

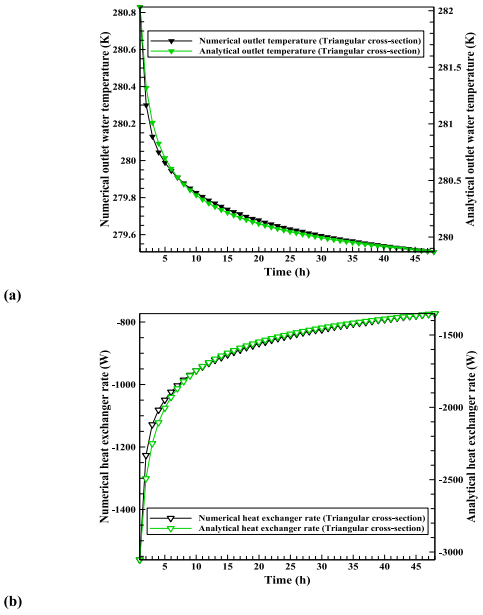


**Fig. 10.** Comparative evaluation of analytical and numerical results for winter HT performance in a triangular U-tube: (a) water $T_{outlet}$ and (b) Heat exchange rate.

rate.

To verify the accuracy of the numerical results, the $T_{outlet}$ and heat exchange rates for the triangular U-tube configuration were carefully compared with analytical solutions using the same thermal conditions and material properties. This validation process was conducted over a continuous 48-h simulation period and is presented in Figs. 10 and 11, corresponding to winter and summer operational modes, respectively.

The comparative analysis reveals a high level of agreement between the numerical and analytical results in both seasonal scenarios. Specifically, the temporal trends and absolute values of $T_{outlet}$ and heat exchange rates obtained from the numerical model closely follow those predicted by the analytical approach, with only minimal deviations observed across the entire simulation window. This strong correlation confirms the accuracy, stability, and predictive capability of the numerical framework used in modeling the GEP system.

Moreover, the validation further substantiates the conclusion that the triangular pipe geometry provides enhanced thermal performance relative to circular and square counterparts. The triangular configuration not only maintains favorable HT characteristics in both heating and cooling modes but also demonstrates consistent behavior across modeling approaches. These findings reinforce its suitability as an efficient and reliable design alternative for optimizing the thermal performance of U-tube HEs embedded in energy piles.

### 4.2. Thermomechanical performance assessment

Fig. 12 illustrates the vertical displacement profiles of GEPs embedded with internal U-tube HEs of circular, square, and triangular cross-sections, each subjected to a concentrated mechanical load of 1,600,000 N. The analysis presented is purely mechanical, excluding thermal influences such as seasonal temperature variations of the circulating fluid during winter and summer. By isolating mechanical effects, this approach enables a focused evaluation of the structural response of the GEP system and offers insight into the role of internal pipe geometry on pile deformation behavior.

The simulation results indicate only minor differences in vertical displacement among the various pipe geometries, suggesting that the internal configuration has a negligible effect on the pile's structural performance under mechanical loading alone. This finding implies that, from a qualitative and design perspective, variations in internal pipe geometry do not pose significant risks in terms of vertical settlement or structural deformation. Consequently, engineers can prioritize thermal performance optimization when selecting pipe geometry, without concern for compromising mechanical integrity or geotechnical safety under standard loading conditions.

At the pile head, downward displacements recorded were 1.762 mm for circular pipe, 1.758 mm for the square pipe, and 1.764 mm for the triangular pipe. These values are nearly identical, indicating negligible differences in load-induced settlement. Similarly, at the pile base, downward displacements were measured at 1.269 mm, 1.266 mm, and 1.270 mm for the circular, square, and triangular configurations, respectively. The near-uniformity in both head and base displacements across all three designs further supports the conclusion that internal pipe geometry does not significantly alter the axial deformation characteristics of the GEP.

Temperature fluctuations inherently induce structural displacements within GEPs due to the combined effects of thermal expansion

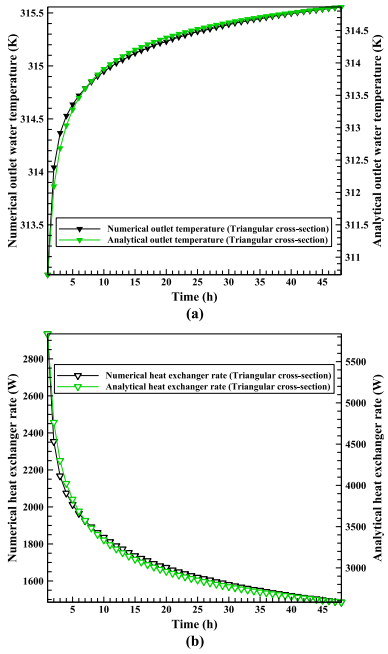


**Fig. 11.** Analytical–numerical comparison of summer HT characteristics in a triangular U-tube: (a) water $T_{outlet}$ and (b) Heat exchange rate.

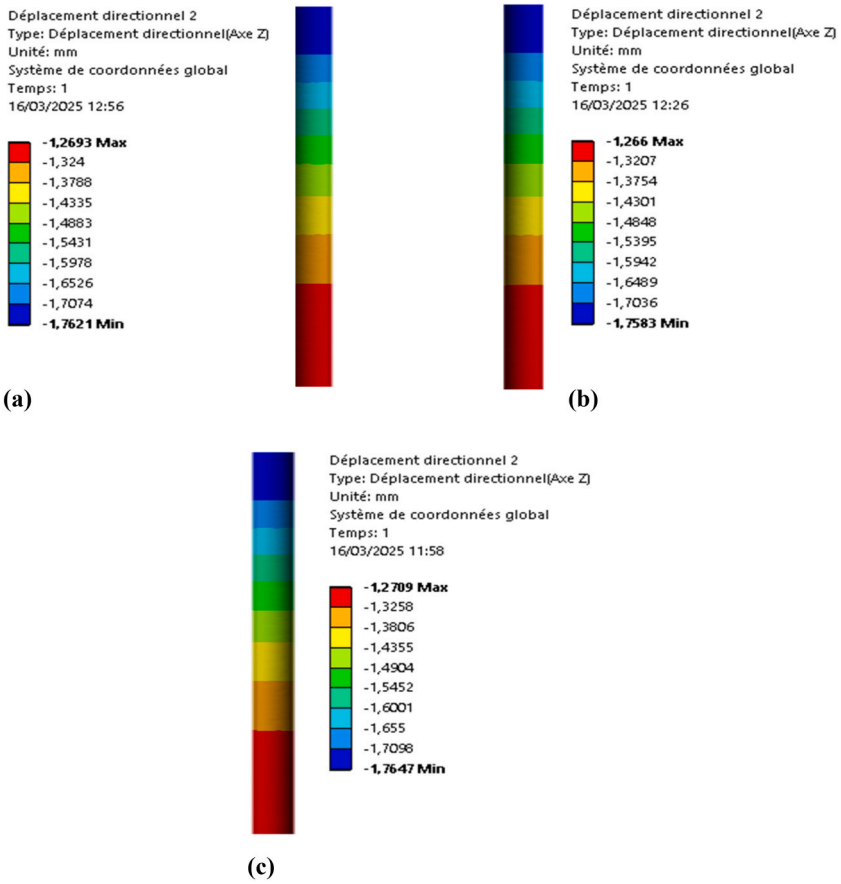


**Fig. 12.** Vertical displacement distribution in GEPs under purely mechanical loading for (a) Circular, (b) Square, and (c) Triangular U-tube configurations.

and mechanical constraints imposed by the surrounding soil. Figs. 13 and 14 illustrate the resulting displacement profiles after 48 h of continuous operation under winter and summer conditions, respectively, for GEP systems embedded with circular, square, and triangular U-tube HEs.

Under winter conditions, as shown in Fig. 13, the displacement behavior reflects the contraction of the pile caused by heat extraction from the surrounding soil. The geometric configuration of the embedded pipe influences the magnitude of this thermally induced deformation. The pile equipped with a circular U-tube experiences a downward displacement of approximately 1.668 mm at the pile head and 1.180 mm at the base. In the case of the square pipe configuration, the displacement are observed at the top of the pile is 1.777 mm, while the displacement at the bottom of the pile is about 1.254 mm. The triangular pipe configuration induces the most pronounced vertical displacement response, with the pile head exhibiting a downward displacement of 1.787 mm and the base displacing downward by 1.256 mm. While the numerical differences compared to other geometries are relatively small, they nonetheless indicate that the triangular geometry, despite its superior thermal efficiency, also leads to slightly greater thermally induced deformation. This suggests a subtle yet important trade-off between enhanced HT performance and structural stability, particularly under cyclic thermal loading. Such behavior may have implications for long-term durability assessments, where repeated temperature fluctuations could cumulatively affect the mechanical integrity of the pile-soil system. Therefore, while the triangular configuration remains advantageous from a thermal standpoint, its structural implications under prolonged operational conditions warrant careful consideration during the design and evaluation of GEP.

As seasonal conditions transition to summer, the thermal behavior of the GEPs shifts accordingly due to the reversal in heat flow direction, from the fluid into the surrounding soil. Fig. 14 illustrates the thermally induced displacement profiles of piles embedded with circular, square, and triangular U-tube HEs after 48 h of continuous cooling-mode operation. During this period, the thermal expansion of the pile becomes the dominant mechanism, resulting from heat injection into the ground. The pile incorporating the circular pipe experiences a downward displacement of approximately 1.748 mm at the top and 1.281 mm at the base. The square configuration yields a nearly identical deformation response, with displacements of 1.742 mm at the top and 1.279 mm at the bottom of the pile. The triangular pipe configuration, consistent with its behavior observed under winter conditions, again shows slightly greater deformation, producing a top (downward) displacement of 1.744 mm and a base (downward) displacement of 1.286 mm. The similarities across these values again confirm that while the differences are minor, the triangular configuration consistently produces

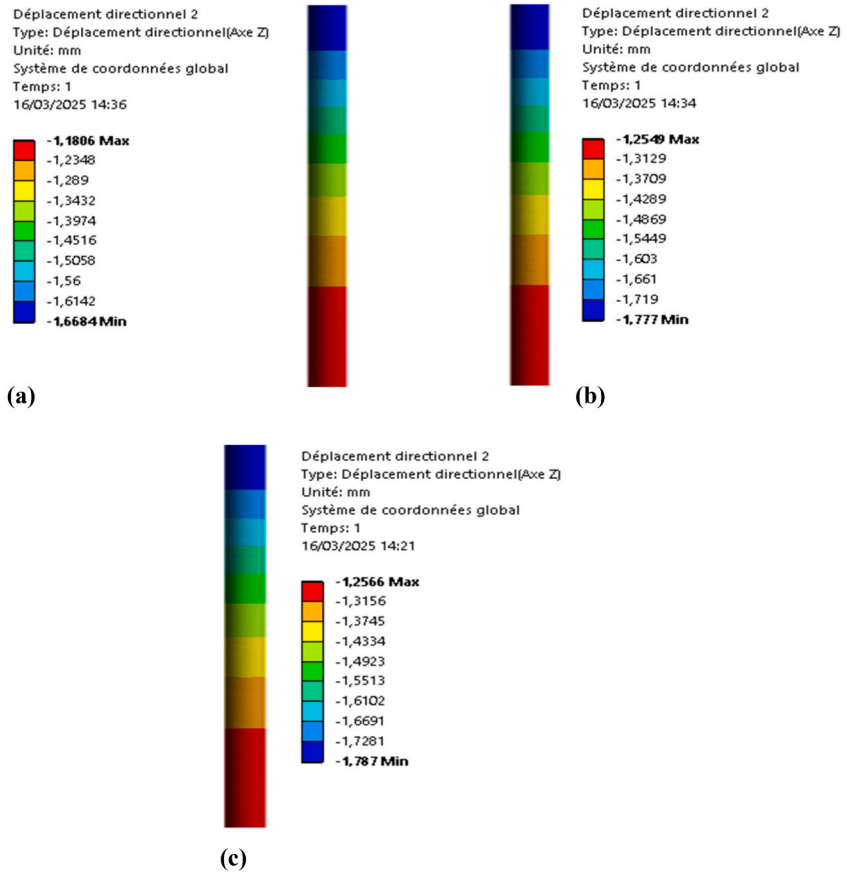


**Fig. 13.** Winter displacement distribution of GEPs under mechanical load and temperature: (a) Circular, (b) Square, and (c) Triangular pipe designs.

slightly greater displacement.

Figs. 15–17 present the displacement distribution profiles along the full length of GEPs subjected to combined thermal–mechanical loading conditions, encompassing both heating (winter) and cooling (summer) phases. These results build upon the thermally induced displacement patterns previously detailed in Figs. 13 and 14, while also incorporating the effects of mechanical loading, as introduced in Fig. 12. For consistency, all analyses were conducted on piles embedded with three distinct U-tube geometries: (a) circular, (b) square, and (c) triangular.

Under purely mechanical loading conditions, the circular pipe configuration exhibits slightly greater basal and vertical displacements than the square configuration, with differences of approximately 0.0033 mm and 0.0039 mm, respectively. In contrast, when compared to the triangular configuration, the circular pipe shows marginally smaller displacements, about 0.0009 mm less at the base and 0.0059 mm less at the pile head. These variations are minimal, suggesting that the influence of internal pipe geometry on the structural response of the pile is minimal when thermal effects are excluded. Accordingly, under mechanical loading alone, all configurations provide comparable structural behavior, reinforcing the conclusion that geometry selection can primarily be guided by thermal performance without compromising mechanical stability.

When thermal effects are introduced under winter conditions, the differences in displacement among pipe configurations become more pronounced. The circular configuration exhibits total displacements at both the base and head of the pile that are lower than those of the square configuration by approximately 0.0744 mm and 0.1082 mm, respectively. However, it still shows slightly smaller displacements compared to the triangular configuration, by about 0.0766 mm at the base and 0.0083 mm at the pile head. This trend indicates that, under heating scenarios, the triangular pipe induces a more substantial thermal response. This is likely attributable to its superior HT characteristics, which enhance thermal interaction with the surrounding soil and result in greater thermally induced expansion or contraction within the pile structure.

In the summer scenario, when the system operates in cooling mode and heat is rejected into the ground, the differences are smaller yet still observable. The circular configuration shows a displacement that greater than the square configuration by about 0.0019 mm at the base of the pile and about 0.0060 mm at the top, while it is less than the triangular configuration by about 0.0073 mm and 0.0044 mm at the base and top of the pile, respectively. These values indicate that even under reversed thermal gradients, the triangular geometry continues to induce slightly greater deformations, although the overall influence of pipe shape on structural displacement remains modest. This behavior, observed across both seasonal conditions, implies a subtle but consistent trade-off between thermal

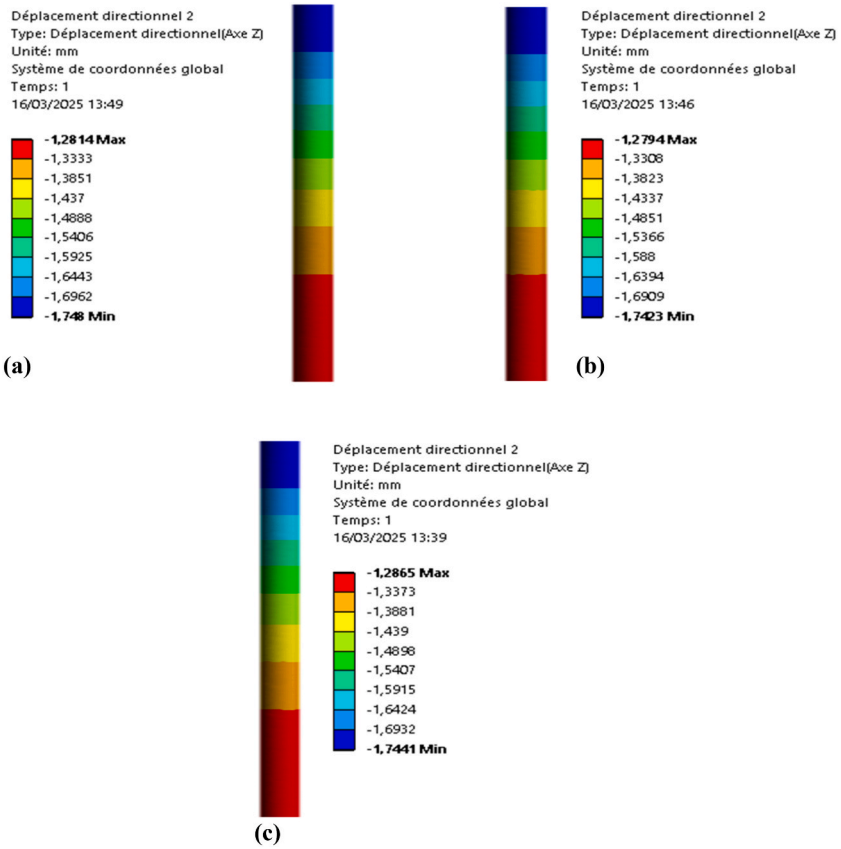


**Fig. 14.** Displacement analysis of energy piles in summer under load and temperature influence: (a) Circular, (b) Square, and (c) Triangular pipe configurations.

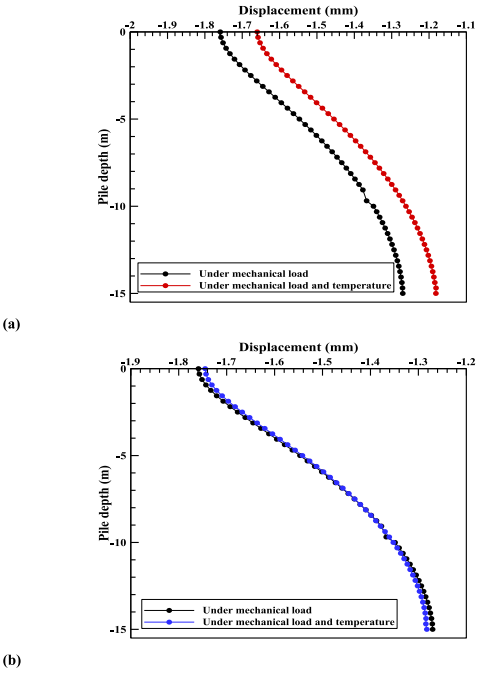


**Fig. 15.** Thermal-induced displacement distribution in GEPs with circular pipe under thermal conditions: (a) Heating and (b) Cooling effects.

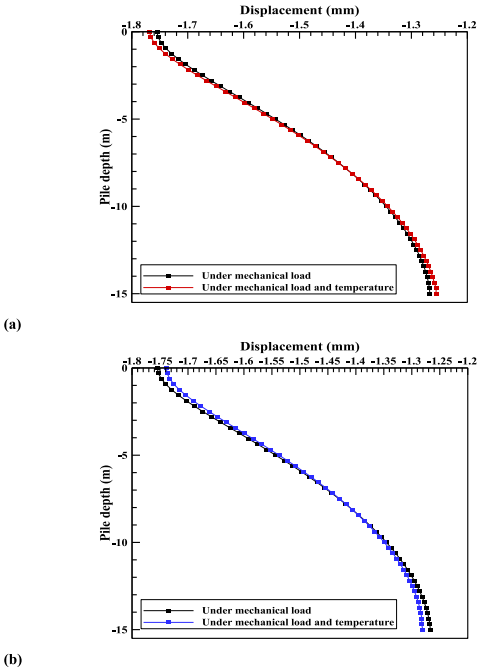


**Fig. 16.** Displacement behavior of energy pile with square GEP under thermal loading: (a) Heating and (b) Cooling.

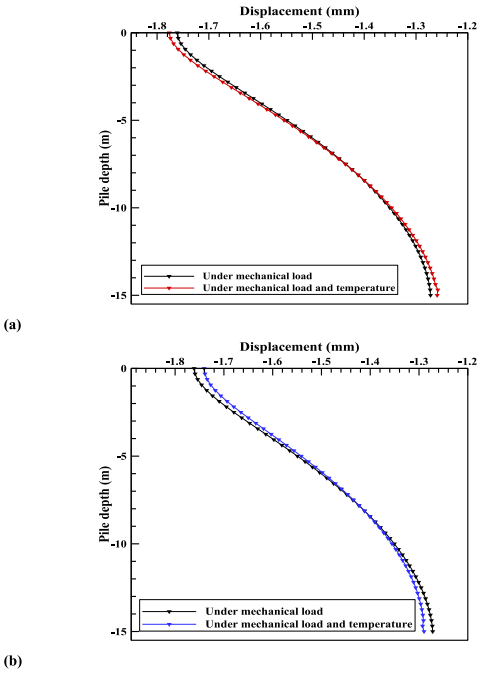


**Fig. 17.** Thermal displacement response of energy pile with triangular GEP: (a) Heating and (b) Cooling.

and structural performance.

The axial stress distribution along the length of GEPs incorporating circular, square, and triangular U-tube HE geometries was analyzed under both purely mechanical and combined thermo-mechanical loading conditions. Figs. 18–20 present the corresponding axial stress profiles for heating (winter) and cooling (summer) operational scenarios. Under the application of a uniform mechanical load of 1,600,000 N, all pile configurations exhibit maximum axial stress at the pile head, the location of the applied external force. The peak axial stresses recorded are 1.5894 MPa for the circular configuration, 1.5872 MPa for the square, and 1.5911 MPa for the

triangular geometry. Despite the identical loading condition, the results underscore the significant influence of pipe geometry on internal stress distribution. The circular geometry, while symmetric, exhibits the highest stress concentration, likely due to its reduced structural stiffness in resisting axial deformation. The square configuration shows slightly lower stress, attributed to its planar surfaces that facilitate a more uniform stress transfer. Meanwhile, the triangular geometry exhibits the lowest peak stress, potentially due to its angular design enhancing stress dissipation along the pile length.

Axial stress gradually decreases along the pile depth, reaching minimum values near the base: 0.0288 MPa for the circular pipe, 0.0253 MPa for the square, and 0.0148 MPa for the triangular pipe. These minimal differences indicate that under purely mechanical loading, the internal pipe shape has little effect on the overall stress distribution within the pile structure. This implies that mechanical stresses are predominantly governed by boundary conditions and global pile geometry.

When thermal effects are introduced, specifically by setting the inlet water temperature to 278.15 K to replicate heating (winter) conditions, the axial stress distribution within the GEPs diverges significantly from that observed under purely mechanical loading. Unlike the uniform axial stress decay seen in the mechanical case, thermal contraction induces compressive stresses that become concentrated around the mid-depth of the pile, with stress magnitudes diminishing progressively toward both the pile head and base. For all pipe geometries, the locations of peak compressive stress are consistent, occurring at approximately 3.7500 m from the pile head. The corresponding maximum compressive stress values are approximately 1.5453 MPa for the circular configuration, 1.6499 MPa for the square, and 1.6667 MPa for the triangular. These findings reveal that the triangular geometry experiences the highest thermally induced axial stress, likely due to its enhanced HT characteristics and the resulting steeper temperature gradients along the pile. This behavior underscores that pipe geometry not only governs the mechanical performance of GEPs but also plays a pivotal role in shaping their thermal stress response under operational heating conditions.

A similar distribution pattern is observed under cooling (summer) conditions, where the inlet water temperature is set to 318.15 K. In this scenario, heat injection into the surrounding soil causes thermal expansion of the pile material, again resulting in the concentration of compressive stresses near the mid-length of the pile. At the same depth identified in the cooling scenario, the stress magnitudes for the circular, square, and triangular configurations are slightly reduced but follow the same relative order, approximately 1.5212 MPa, 1.5107 MPa, and 1.4899 MPa, respectively. This mid-depth stress concentration can be attributed to the interaction between thermal expansion or contraction and the geometric constraints imposed by the surrounding soil, which limits axial displacement and results in localized stress accumulation. The triangular configuration consistently exhibits the highest stress values, likely due to stress intensification at its angular corners, whereas the circular configuration shows the lowest, indicating a more uniform stress distribution. This persistent mid-depth stress localization identifies the central region of the pile as the most susceptible to thermally induced deformation, regardless of whether the pile is operating in heating or cooling mode.

In the numerical simulation of pile foundations, the shear interaction at the pile–soil interface is modeled as frictional resistance, effectively capturing the mobilization of shear stress under both mechanical and thermal influences. This approach allows for an accurate representation of soil–structure interaction, particularly under varying loading conditions. Within this simulation framework, three pile geometries, circular, square, and triangular, were investigated to assess how shear stress develops along the pile depth. The corresponding distributions, presented in Figs. 21–23, illustrate the behavior of each configuration under a purely mechanical load of 1,600,000 N, as well as under combined thermal–mechanical loading during both heating and cooling phases.

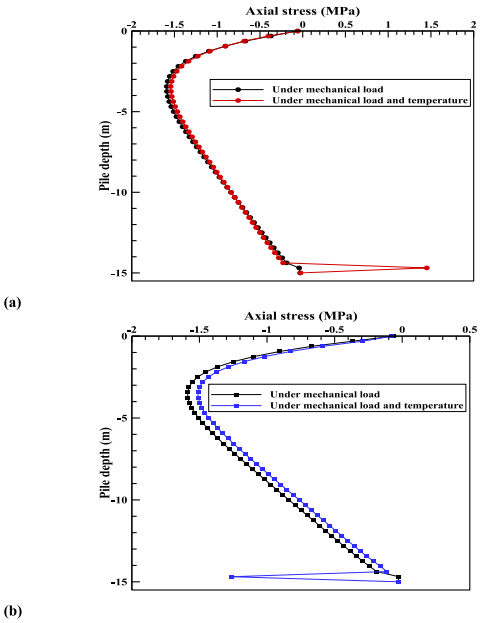


**Fig. 18.** Axial stress response in energy pile with circular GEP during thermal exposure: (a) Heating and (b) Cooling.

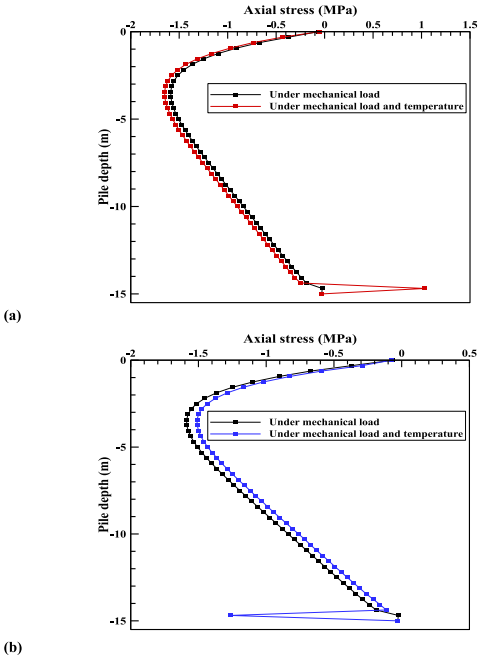


**Fig. 19.** Shear stress behavior in energy pile with square GEP during thermal loading: (a) Heating and (b) Cooling.

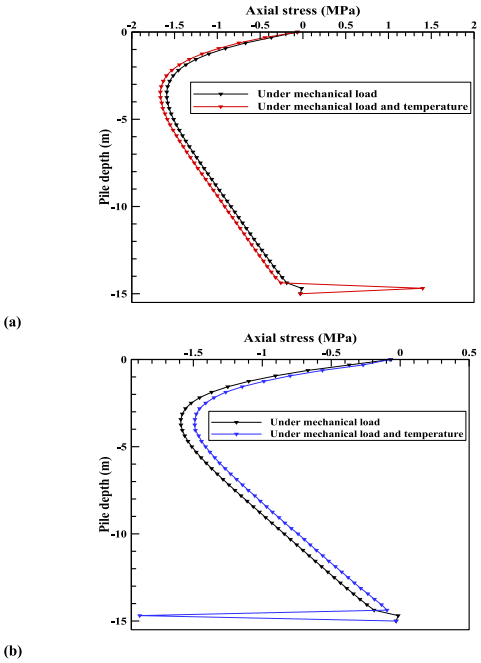


**Fig. 20.** Thermal-induced axial stress distribution in energy pile with triangular pipe: (a) Heating and (b) Cooling.

A consistent pattern was observed across all pipe configurations and loading scenarios: shear stress is predominantly concentrated within the upper 3.7500 m of the pile. This upper segment represents the primary zone of pile–soil interaction, where frictional resistance is maximized due to elevated normal stresses and stronger confinement near the ground surface. As depth increases, shear stress gradually decreases, reflecting reduced contact pressure and diminished relative displacement between the pile and surrounding soil. This distribution underscores that the efficiency of shear load transfer is strongly influenced by near-surface soil stiffness and confinement, both of which decline with depth. Consequently, the upper portion of the pile functions as the principal load-transfer

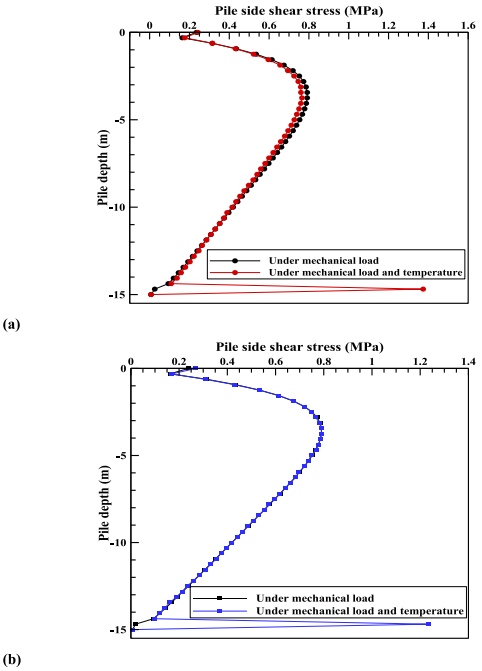


**Fig. 21.** Shear stress distribution of GEP with circular pipe: (a) Heating and (b) Cooling.

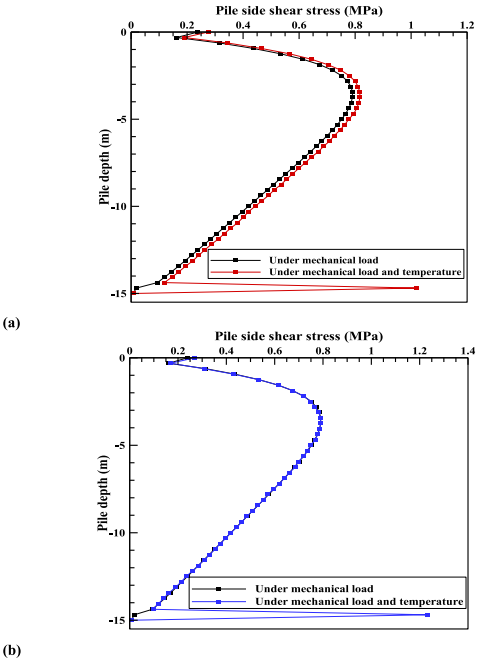


**Fig. 22.** Thermal-dependent shear stress distribution in GEP with square pipe: (a) Heating and (b) Cooling.

interface, while deeper segments contribute less to shear resistance due to the combined effects of lower normal stress and weaker soil–pile adhesion.

Thermal effects play a pivotal role in modulating these shear stress patterns. During heating (simulated with elevated inlet fluid temperatures), thermal expansion of the pile slightly increases lateral pressure against the soil, enhancing contact friction in the upper regions. Conversely, cooling induces thermal contraction, which reduces the pile's outward pressure on the soil, thereby lowering the interface shear stress, especially at greater depths. These thermally induced deformations subtly reshape the internal stress

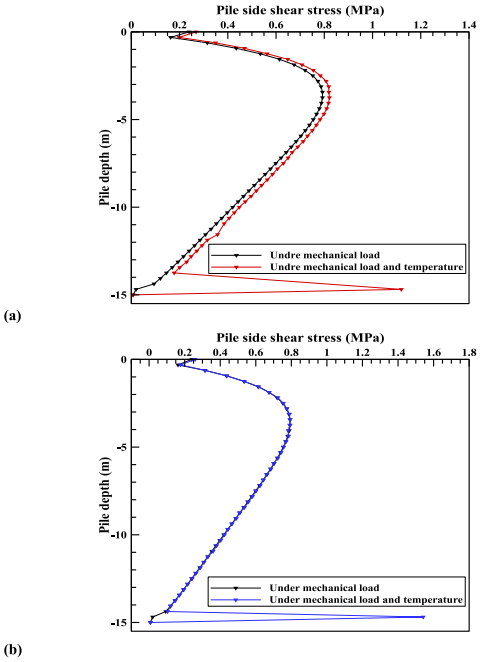


**Fig. 23.** Shear stress behavior in GEP with triangular pipe during (a) Heating and (b) Cooling.

distribution, intensifying shear mobilization near the top while decreasing it toward the base.

The abrupt changes in shear stress observed near the bottom of the pile in Figs. 21–23 under combined thermal and mechanical loading, during both heating and cooling phases, can be directly linked to the specific configuration of the embedded HE system. Notably, the thermal pipe does not extend the full length of the pile, terminating approximately 0.5 m above the pile base. Consequently, the lower segment of the pile remains thermally inactive, experiencing negligible temperature-induced expansion or contraction. This design discontinuity introduces a distinct interface between thermally active and inactive zones, giving rise to a strain incompatibility along the pile length. The resulting differential thermal deformation induces localized internal stress adjustments, which manifest as sharp variations in shear stress at this transitional region.

Furthermore, the pile base typically encounters increased mechanical constraint due to its interaction with a stiffer underlying soil layer or bedrock, which restricts vertical displacement and exacerbates stress accumulation. This boundary condition further amplifies the redistribution of stresses near the pile tip, intensifying the observed shear stress gradients. Therefore, the combined effects of the thermal system's geometric limits and the mechanical boundary conditions at the pile base account for the pronounced shear stress discontinuities in this region.

## 5. Conclusions

This study presents a comprehensive numerical investigation into the thermomechanical performance of GEPs incorporating U-shaped HE pipes of varying cross-sectional geometries, namely circular, square, and triangular, under seasonal (summer and winter) operating conditions. The simulations, conducted using ANSYS Fluent 20.0, offer important insights into the coupling between thermal behavior and mechanical stability within GEP systems. The key findings can be summarized as follows:

Geometric configuration significantly governs HE performance: The shape of the embedded U-pipes plays a crucial role in defining the overall HT performance. Analytical formulations combined with numerical simulations confirm that the geometry of the HE directly influences thermal conductivity paths and fluid-solid interaction, thereby affecting system efficiency. Over 48-h operational cycles in both summer (cooling) and winter (heating), notable differences were observed across the tested configurations.

Seasonal thermal trends follow physically intuitive behavior: In summer, the fluid temperature at the outlet ($T_{outlet}$) decreases as thermal energy is absorbed by the surrounding soil, which in turn leads to a progressive increase in soil temperature along the pile depth. Conversely, in winter, the fluid gains heat from the soil, raising the $T_{outlet}$ while inducing a decline in soil temperature. These opposite gradients affirm the dual-mode energy exchange capacity of GEPs and support the seasonal reversibility of HT.

Triangular pipe geometry exhibits superior cooling performance: Among the three configurations studied, the triangular U-pipe delivered the best thermal performance under cooling loads, showing a $T_{outlet}$ reduction of approximately 1.206 K and 1.598 K relative to circular and square pipes, respectively. It also demonstrated enhanced heat extraction capacity, with gains of 45.727 W and 163.627 W over the other shapes. However, in heating conditions, although the triangular pipe provided higher fluid outlet temperatures (0.629 K and 0.836 K higher than circular and square, respectively), it exhibited slightly reduced HT rates (by 25.416 W and 111.03 W). These results emphasize the need for season-specific design considerations or hybrid configurations that balance performance

across varying operational modes.

The superior thermal performance of the triangular pipe configuration during cooling mode can be attributed to its angular geometry, which induces flow separation and promotes the formation of secondary circulations within the pipe. These internal flow disturbances enhance convective HT by disrupting the thermal boundary layer and increasing turbulence intensity near the pipe walls. Additionally, the triangular cross-section facilitates tighter fluid contact at the corners, effectively increasing the active heat exchange surface area. In contrast, while the square configuration possesses a relatively high perimeter-to-area ratio, which theoretically favors HT, it tends to experience flow stagnation and recirculation zones in its corners. These low-velocity regions hinder effective convective transport, thereby reducing the overall HT efficiency.

Simulation results are consistent with theoretical expectations: The temperature profiles and heat flux predictions obtained from the numerical model for the triangular configuration closely match theoretical estimates, indicating that the developed simulation framework reliably captures the underlying thermophysical behavior when subjected to realistic boundary and loading conditions.

Mechanical behavior follows geotechnical principles under axial load: Under static mechanical loading, axial compressive stress decreases linearly from the pile head to its base, while the vertical displacement follows an inverse trend, maximum at the base and minimum at the top, consistent with classical axial loading theory in pile foundations.

Coupled thermomechanical loading alters deformation characteristics: Under simultaneous thermal and mechanical loading scenarios, the displacement profile maintains linearity across the pile depth. The bottom of the pile experiences the greatest deflection, though the overall structural integrity remains within acceptable safety margins. This suggests the robustness of GEPs when exposed to real-world multi-physical interactions.

Thermally induced stress distributions are shape-sensitive: Seasonal thermal expansion and contraction result in characteristic axial and shear stress patterns, with maximum stress typically concentrated near the mid-depth of the pile. The magnitude and spatial distribution of these stress fields are notably influenced by pipe geometry, underlining the need to factor thermal stress concentrations into structural design to avoid fatigue or failure over time.

Compared to the purely mechanical loading scenario for each pipe geometry, the mechanical behavior of the GEPs under thermo-mechanical coupling in summer conditions reveals a noticeable increase in axial compressive stress. Specifically, the circular, square, and triangular configurations exhibit increases of approximately 4.29 %, 4.82 %, and 6.36 %, respectively. This stress amplification is primarily driven by thermal contraction of the pile material induced by internal cooling, which adds to the existing mechanical load. Conversely, under winter heating conditions, axial compressive stresses are reduced relative to the mechanical-only case, with decreases of about 2.77 % for the circular configuration, 3.95 % for the square, and 4.75 % for the triangular. These reductions result from thermal expansion counteracting the applied mechanical load, partially relieving stress along the pile length.

Displacement distributions at the pile base also reflect the influence of thermal effects, though with less pronounced variation across geometries. In summer, the circular, square, and triangular piles exhibit slight decreases in base displacement of 0.57 %, 1.14 %, and 1.13 %, respectively, compared to the conventional load case. In contrast, during winter heating, the same configurations show increased base displacements of 5.11 %, 1.13 %, and 1.70 %, respectively.

The interplay between pipe geometry, internal flow behavior, and soil–structure interaction underscores that optimizing GEP performance extends beyond maximizing thermal efficiency. For instance, the triangular configuration demonstrates superior cooling performance due to enhanced internal fluid turbulence and sharper thermal gradients concentrated along its angular boundaries. However, these thermal advantages come with trade-offs: elevated thermally induced stresses and larger structural displacements, which may compromise long-term mechanical integrity. This duality highlights the importance of integrated design strategies that balance thermal performance with structural resilience in energy pile systems.

Building upon the outcomes of this study, several avenues for future research are proposed:

(i) Investigate more complex or hybrid cross-sectional shapes (e.g., elliptical, hexagonal) to identify configurations that optimize HT and structural performance across seasons;
(ii) Incorporate real climatic and operational data: Use long-term field temperature profiles and seasonal ground conditions to simulate realistic thermal cycles and assess soil thermal recovery and fatigue;
(iii) Analyze the influence of variable soil types, moisture migration, and groundwater flow on thermal efficiency and mechanical stability;
(iv) Conduct experimental studies or pilot installations to verify simulation results and adjust modeling parameters based on observed data;
(v) Conduct life-cycle cost analysis to evaluate the economic viability of different pipe shapes in terms of energy savings and installation costs.

## CRediT authorship contribution statement

**Samia Boudjaza:** Writing – original draft, Software, Investigation, Conceptualization. **Abdelmadjid Chehhat:** Methodology, Investigation, Formal analysis, Data curation. **Abdelmadjid Kaddour:** Writing – review & editing, Validation, Resources, Conceptualization. **Younes Menni:** Writing – review & editing, Supervision, Methodology, Formal analysis. **Samia Larguech:** Writing – review & editing, Supervision, Methodology, Conceptualization. **Badr M. Alshammari:** Writing – review & editing, Visualization, Validation, Software. **Lioua Kolsi:** Writing – review & editing, Methodology, Investigation, Conceptualization.

## Declaration of competing interest

The authors declare that they have no known competing financial interests or personal relationships that could have appeared to influence the work reported in this paper.

## Acknowledgements

Princess Nourah bint Abdulrahman University Researchers Supporting Project number (PNURSP2025R826), Princess Nourah bint Abdulrahman University, Riyadh, Saudi Arabia.

## Data availability

Data will be made available on request.

## References

[1] H. Wang, B.W. Ang, B. Su, A multi-region structural decomposition analysis of global $CO_2$ emission intensity, Ecol. Econ. 142 (2017) 163–176, https://doi.org/10.1016/j.ecolecon.2017.06.023.
[2] M. Merdassi, M. Aouissi, Numerical simulation and comparative analysis of Earth air heat exchanger designs, Int. J. Heat Technol. 42 (6) (2024) 2143–2156, https://doi.org/10.18280/ijht.420633.
[3] A.K. Sani, R.M. Singh, T. Amis, I. Cavarretta, A review on the performance of geothermal energy pile foundation, its design process and applications, Renew. Sustain. Energy Rev. 106 (2019) 54–78, https://doi.org/10.1016/j.rser.2019.02.008.
[4] I.A. Gondal, S.A. Masood, M. Amjad, Review of geothermal energy development efforts in Pakistan and way forward, Renew. Sustain. Energy Rev. 71 (2017) 687–696, https://doi.org/10.1016/j.rser.2016.12.097.
[5] A.K. Sani, R.M. Singh, I. Cavarretta, S. Bhattacharya, Heat storage performance of a pile heat exchanger installed in partially saturated swelling clay, in: The 7th International Conference on Unsaturated Soils, 2018, August, pp. 1–6. https://www.issmge.org/publications/online-library.
[6] D. Banks, An Introduction to Thermogeology: Ground Source Heating and Cooling, John Wiley & Sons, 2012, https://doi.org/10.1002/9781118447512.
[7] A.K. Sani, R.M. Singh, Response of unsaturated soils to heating of geothermal energy pile, Renew. Energy 147 (2020) 2618–2632, https://doi.org/10.1016/j.renene.2018.11.032.
[8] M.Y. Fattah, B.S. Zbar, F.S. Mustafa, Effect of soil saturation on load transfer in a pile excited by pure vertical vibration, Proceedings Institut. Civil Eng. Struct. Build. 174 (2) (2021) 132–144, https://doi.org/10.1680/jstbu.16.00206.
[9] M.Y. Fattah, R.R. Al-Omari, S.H. Fadhil, Load sharing and behavior of single pile embedded in unsaturated swelling soil, European J. Environmental Civil Eng. 24 (12) (2020) 1967–1992, https://doi.org/10.1080/19648189.2018.1495105.
[10] M.Y. Fattah, B.S. Zabar, F.S. Mustafa, Effect of saturation on response of a single pile embedded in saturated sandy soil to vertical vibration, European J. Environmental Civil Eng. 24 (3) (2020) 381–400, https://doi.org/10.1080/19648189.2017.1391126.
[11] W. Huang, H. Li, G. Sun, D. Jiang, Y. Gao, Performance research of materials and engineering application of overburden strata separation-zone grouting technology, Adv. Mater. Sci. Eng. 2022 (1) (2022) 3513993, https://doi.org/10.1155/2022/3513993.
[12] P. Zhang, M. Liu, Z. Li, Q. Lv, Z. Sun, Q. Zhang, X. Liu, Simulation and analysis of the thermal-mechanical response of an energy pile, Lithosphere 2022 (Special 10) (2022) 5506908, https://doi.org/10.2113/2022/5506908.
[13] Q. Zhao, B. Chen, F. Liu, Study on the thermal performance of several types of energy pile ground heat exchangers: U-Shaped, W-shaped and spiral-shaped, Energy Build. 133 (2016) 335–344, https://doi.org/10.1016/j.enbuild.2016.09.055.
[14] X. Li, H. Guo, X. Cheng, Experimental and numerical study on temperature distribution in energy piles, China Civ. Eng. J. 49 (4) (2016) 102–110.
[15] A.H. Farajollahi, B. Asgari, M. Rostami, Thermal performance analysis of an energy pile with triple helix ground heat exchanger, Geothermics 104 (2022) 102459, https://doi.org/10.1016/j.geothermics.2022.102459.
[16] Y. Rui, K. Soga, Thermo-hydro-mechanical coupling analysis of a thermal pile, Proceedings Institution Civil Eng. Geotech. Eng. 172 (2) (2019) 155–173, https://doi.org/10.1680/jgeen.16.00133.
[17] F. Cecinato, D. Salciarini, Energy performance assessment of thermo-active micro-piles via numerical modeling and statistical analysis, Geomech. Energy Environment 29 (2022) 100268, https://doi.org/10.1016/j.gete.2021.100268.
[18] S. Lee, S. Park, D. Ahn, H. Choi, Thermal performance of novel cast-in-place energy piles equipped with multipurpose steel pipe heat exchangers (SPHXs), Geothermics 102 (2022) 102389, https://doi.org/10.1016/j.geothermics.2022.102389.
[19] S. Park, S. Lee, D. Lee, D. Ahn, H. Choi, Effect of thermal interference on energy piles considering various configurations of heat exchangers, Energy Build. 199 (2019) 381–401, https://doi.org/10.1016/j.enbuild.2019.07.008.
[20] A.A. Mehrizi, S. Porkhial, B. Bezyan, H. Lotfizadeh, Energy pile foundation simulation for different configurations of ground source heat exchanger, Int. Commun. Heat Mass Tran. 70 (2016) 105–114, https://doi.org/10.1016/j.icheatmasstransfer.2015.12.001.
[21] S. Shahidi, M. Hajialilue-Bonab, H.R. Tohidvand, A. Khosravi, Experimental investigation on the efficiency of the phase change materials for enhancing the thermal performance of energy piles in sandy soils, Energy Build. 298 (2023) 113544, https://doi.org/10.1016/j.enbuild.2023.113544.
[22] Y. Guo, C. Wang, A. Bouazza, H. Chang, G. Kong, Thermal performance of a full-scale pre-tensioned high strength concrete (PHC) energy pile, J. Energy Storage 98 (2024) 112840, https://doi.org/10.1016/j.est.2024.112840.
[23] M. Liu, P. Zhang, Z. Yang, Z. Zhu, X. Liu, C. Ma, Study on thermodynamic properties of spiral tube-encapsulated phase-change material energy pile, Buildings 14 (1) (2024) 188, https://doi.org/10.3390/buildings14010188.
[24] X. Bao, Y. Li, T. Feng, H. Cui, X. Chen, Investigation on thermo-mechanical behavior of reinforced concrete energy pile with large cross-section in saturated sandy soil by model experiments, Undergr. Space 5 (3) (2020) 229–241, https://doi.org/10.1016/j.undsp.2019.03.009.
[25] Y. Lou, P.F. Fang, X.Y. Xie, R.H. Zhang, C.S.A. Chong, Z.J. Wang, D.Y. Zhu, Experimental study on thermo-mechanical responses of pre-bored grouted planted piles with different restraint conditions, Energy Build. 268 (2022) 112232, https://doi.org/10.1016/j.enbuild.2022.112232.
[26] C. Han, X.B. Yu, Analyses of the thermo-hydro-mechanical responses of energy pile subjected to non-isothermal heat exchange condition, Renew. Energy 157 (2020) 150–163, https://doi.org/10.1016/j.renene.2020.04.118.
[27] A. Moradshahi, M. Faizal, A. Bouazza, J.S. McCartney, Cross-sectional thermo-mechanical responses of energy piles, Comput. Geotech. 138 (2021) 104320, https://doi.org/10.1016/j.compgeo.2021.104320.
[28] T. Du, Y. Li, X. Bao, W. Tang, H. Cui, Thermo-mechanical performance of a phase change energy pile in saturated sand, Symmetry 12 (11) (2020) 1781, https://doi.org/10.3390/sym12111781.
[29] H. Chang, G. Kong, H. Liu, Estimation of the technical geothermal potential through energy piles at a small regional scale: a campus case study, Energy 320 (2025) 135290, https://doi.org/10.1016/j.energy.2025.135290.
[30] M.A. Baffa, Z. Mustaffa, N.R. Ahmad, M.E. El-Atroush, N.S.A. Yaro, M.E.A.B. Seghier, Performance of geothermal energy piles in buildings: a bibliometric analysis and systematic review, Energy Build. (2025) 115357, https://doi.org/10.1016/j.enbuild.2025.115357.

[31] Y.Z. Zhao, Z. Shi, Z.Y. Ai, Time-dependent behaviors of pile groups in geothermal heat exchangers, Renew. Sustain. Energy Rev. 213 (2025) 115485, https://doi.org/10.1016/j.rser.2025.115485.
[32] M. Fattahian, M.H. Sobhdam, M.M. Ahmadi, O. Ghasemi-Fare, Comparison of mixed convection effects in summer and winter on the energy efficiency of energy piles, Renew. Energy 248 (2025) 123138, https://doi.org/10.1016/j.renene.2025.123138.
[33] A. Lupattelli, D. Salciarini, Investigating the impact of temperature recovery across different thermal activation scenarios of a real-world energy piled foundation, Tunn. Undergr. Space Technol. 158 (2025) 106457, https://doi.org/10.1016/j.tust.2025.106457.
[34] H. Song, L. Zheng, Z.J. Cao, K. Cui, H. Pei, W. Liu, S. Zhang, Thermomechanical analysis of dissimilar energy pile groups using a load transfer method, Renew. Energy (2025) 123708, https://doi.org/10.1016/j.renene.2025.123708.
[35] C. Wang, S. Dong, A. Bouazza, X. Ding, Explainable machine learning models to predict outlet water temperature of pipe-type energy pile, Renew. Energy 246 (2025) 122972, https://doi.org/10.1016/j.renene.2025.122972.
[36] J. Yuan, Z. Chen, H. Xiao, L. Zheng, W. Li, X. Song, Thermal-mechanical behavior of deeply buried pipe energy pile group in sand obtained from model test, Appl. Therm. Eng. 261 (2025) 125078, https://doi.org/10.1016/j.applthermaleng.2024.125078.
[37] U.C. Erginag, M. Guner, S. Polat, M. Sutman, O. Cinicioglu, Thermally induced tensile hoop stresses in energy piles: implications for design and operation, Geomech. Energy Environment (2025) 100702, https://doi.org/10.1016/j.gete.2025.100702.
[38] C. Hu, J. Cui, M. Wang, Y. Zhang, J. Luo, L. Li, Optimizing the restoration performance of pipe energy piles using energy injection in winter mode: a numerical investigation, J. Energy Storage 114 (2025) 115807, https://doi.org/10.1016/j.est.2025.115807.
[39] Q.I. Alqawasmeh, M.J. Kreitmair, G.A. Narsilio, The role of ground hydrothermal spatial variability on energy pile group thermal performance, Comput. Geotech. 179 (2025) 106983, https://doi.org/10.1016/j.compgeo.2024.106983.
[40] C. Liu, J. Li, P. Zhou, G. Liu, P. Li, Thermo-hydro-mechanical behavior of energy piles in partially saturated soils: a theoretical prediction approach, Comput. Geotech. 185 (2025) 107332, https://doi.org/10.1016/j.compgeo.2025.107332.
[41] F. He, H. Liu, C. Wang, A. Bouazza, G. Kong, Z. Sun, Effects of thermal loading conditions on the thermo-mechanical response of energy pile at different depths, Geothermics 131 (2025) 103392, https://doi.org/10.1016/j.geothermics.2025.103392.
[42] P.Z. Zhuang, K.X. Wang, X.G. Song, X. Geng, H. Yang, Thermo-mechanical behaviour of energy pile considering non-uniform initial ground temperatures, Proceedings Institution Civil Eng. Geotech. Eng. (2025) 1–23, https://doi.org/10.1680/jgeen.24.00363.
[43] C. Hu, H. Gu, J. Luo, D. Tian, Numerical study on heat restoration cycle performance of energy pile with backfilling PCM, Case Stud. Therm. Eng. 61 (2024) 105047, https://doi.org/10.1016/j.csite.2024.105047.
[44] H. Zhao, C. Wang, G. Kong, X. Ding, An approach for analysis of a single energy pile subjected to a horizontal load in sand, Case Stud. Therm. Eng. 56 (2024) 104289, https://doi.org/10.1016/j.csite.2024.104289.
[45] C. Xu, Y. Wang, X. Meng, Q. Lv, H. Chen, Q. Wu, A multiphysics simulation study of the thermomechanical coupling response of energy piles, Buildings 14 (5) (2024) 1440, https://doi.org/10.3390/buildings14051440.
[46] B.E. Launder, D.B. Spalding, The numerical computation of turbulent flows, Comput. Methods Appl. Mech. Eng. 3 (2) (1974) 269–289, https://doi.org/10.1016/0045-7825(74)90029-2.
[47] ANSYS Inc, ANSYS Europe Ltd, ANSYS fluent user's guide. Release 2020 R2. July 2020. https://www.scribd.com/document/478910198/ANSYS-Fluent-Tutorial-Guide-2020-R2-pdf, 2020.
[48] S.V. Patankar, Numerical Heat Transfer and Fluid Flow, McGraw-Hill, New York, 1980, https://doi.org/10.1201/9781482234213.

## Nomenclature

*A:* Cross-sectional area of the pile ($m^2$)
$\mathbf{C_{\epsilon 1}}, \mathbf{C_{\epsilon 2}}$*:* Empirical constants for the turbulence model
$\mathbf{C_\mu}$: Empirical constant for turbulent viscosity
$\mathbf{c_p}$: Specific heat capacity ($J.kg^{-1}.K^{-1}$)
δ: Displacement (m)
$\Delta\mathbf{l}$: Distance between strain points i and i-1 (m)
$\Delta\mathbf{T}$: Temperature change (K)
**E**: Young's modulus of the pile material (Pa)
ε: Dissipation rate of turbulence kinetic energy ($J.kg^{-1}.s^{-1}$)
$\boldsymbol{\epsilon}$: Strain
$\boldsymbol{\epsilon}_{res}$: Residual strain
$\boldsymbol{\epsilon}_{\mathbf{T}}$: Thermal strain
$\boldsymbol{\epsilon}_{\mathbf{T-free}}$: Free thermal strain
**F**: Axial load applied to the pile (N)
$\mathbf{G_k}$: Production rate of turbulence kinetic energy ($J.kg^{-1}.s^{-1}$)
**k**: Turbulence kinetic energy ($m^2.s^{-2}$)
λ: Thermal conductivity ($W.m^{-1}.K^{-1}$)
$\lambda_s$: Thermal conductivity of the solid ($W.m^{-1}.K^{-1}$)
**L**: Length of the pile (m)
μ: Dynamic viscosity ($kg.m^{-1}.s^{-1}$)
$\mu_t$: Turbulent viscosity (Pa.s)
ν: Kinematic viscosity of the fluid ($m^2.s^{-1}$)
**P**: Pressure ($N.m^{-2}$)
$\nabla\mathbf{p}$: Pressure gradient ($Pa.m^{-1}$)
**Q**: Heat flux ($W.m^{-2}$)
**q**: Internal heat generation flux in the solid ($W.m^{-2}$)
$\mathbf{q_r}$: Radiative heat flux ($W.m^{-2}$)
ρ: Density ($kg.m^{-3}$)
σ: Axial temperature stress ($N.m^{-2}$)
$\sigma_{res}$: Residual axial stress ($N.m^{-2}$)
$\sigma_\mathbf{k}, \sigma_\varepsilon$: Turbulent Prandtl numbers
**t**: Time (s)
**T**: Temperature (K)
τ: Stress tensor (Pa)
**u**: Fluid velocity ($m.s^{-1}$)
$\mathbf{u}_{trans}$: Translational velocity of the solid ($m.s^{-1}$)
**U**: Velocity component ($m.s^{-1}$)
**x**: Spatial coordinate (m)
$\nabla\mathbf{T}$: Temperature gradient ($K.m^{-1}$)
$\nabla\mathbf{u}$: Velocity gradient ($s^{-1}$)

$\boldsymbol{\phi}$: Dissipation function ($W.m^{-3}$)
$\alpha$: Coefficient of thermal expansion ($K^{-1}$)

## Subscripts

*f:* Fluid
*i, j:* Indices representing spatial directions
*mech:* Mechanical
*r:* Radiant
*res:* Residual
*s:* Solid
*trans:* Translational

## Abbreviation

*CFD:* Computational fluid dynamics
*FF:* Fluid flow
*FVM:* Finite volume method
*GE:* Geothermal energy
*GEP:* Geothermal energy pile
*GTP:* Geothermal thermal pile
*HCF:* Heat carrier fluid
*HDPE:* High density polyethylene
*HE:* Heat exchanger
*HT:* Heat transfer
*PCM:* Phase change material
*PHC:* Pre-tensioned high-strength concrete
*PISO:* Pressure implicit with splitting of operators
*PGP:* Pre-bored grouted planted
*SOU:* Second order upwind
*TRTs:* thermal response tests